Heterogeneous ceramic interfaces in solid oxide fuel cells and dense oxygen permeable membranes

Sonia Faaland

A thesis in partial fulfilment
of the requirements for the
Norwegian academic degree

Doktor ingeniør

Department of Chemistry
Norwegian University of Science and Technology

October 2000

Abstract

Solid oxide fuel cells and oxygen permeable membranes have received considerable attention during the last decade due to the increasing demand for electrical energy and easily transportable fuels combined with the requirement of low emission of CO_2. This work concentrates on the stability of ceramic interfaces in general, and more specifically to heterophase solid state interfaces related to solid oxide fuel cells and oxygen permeable membranes. Reaction mechanisms are discussed and requirements and properties of suitable materials are determined. This thesis consists of three parts: 1) Structure of Ca-substituted lanthanum manganite (Paper I), 2) Reactions between cathode and electrolyte for SOFC applications (Papers II-IV) and 3) Chemical and mechanical aspects of sealing dense oxygen permeable membranes (Papers V and VI).

Calcium-substituted lanthanum manganite, $La_{1-x}Ca_xMnO_3$ (LCM), is a promising material for high temperature solid oxide fuel cell cathodes because of its high electrical conductivity and good compatibility with cubic stabilized zirconia. In paper I we report on the structure of $La_{1-x}Ca_xMnO_3$ (x=0.2, 0.3, 0.4, 0.6) studied by synchrotron X-ray powder diffraction, electron diffraction and IR spectroscopy. The structure refinement reveals an orthorhombic crystal structure with space group Pnma. A strong correlation was observed between the cooling rate from calcination temperature and the powder quality, indicating the importance of a homogeneous oxygen stoichiometry.

The chemical stability of the interface between LCM and cubic calcia stabilized zirconia (CSZ) has been studied in papers II-IV as a model system for the cathode and the electrolyte in solid oxide fuel cells. The formation of secondary phases was observed to depend on the composition of the manganite and the partial pressure of oxygen. The most chemically stable interface was observed when the lanthanum manganite contained 30 mole% calcium on La-site both in air and in reducing atmosphere ($pO_2 \sim 10^{-6}$ atm). Even on a nano-meter scale, there were no indications of secondary phases in $La_{0.7}Ca_{0.3}MnO_3$/CSZ powder mixtures fired in air. Reducing atmosphere was observed to destabilize the interface. A-site deficiency of the lanthanum manganite, however, was observed to increase the kinetic and thermodynamic stability. The experimental findings in papers II-IV are discussed in relation to the stability of the cathode / electrolyte interface of conventional solid oxide fuel cells, consisting of strontium substituted

lanthanum manganite and yttria stabilized zirconia (Papers VII-VIII).

In paper V we have studied the chemical stability of the interface between $La_{1-x}(Ca,Sr)_xCoO_3$ and $CaSiO_3$ / Ca_2SiO_4 as a simplified model for the interface between membrane and sealant in dense oxygen permeable membrane systems. Sintered powder mixtures of the two materials were analyzed to gain information about coexistent equilibrium phases in the CaO / SrO - La_2O_3 - CoO - SiO_2 system. The estimated phase composition along the $CaSiO_3$ - $LaCoO_3$ line has been worked out. Strontium substituted lanthanum cobaltite was observed to give rise to the highest thermodynamic stability of a perovskite phase. The chemical aspects of glass-ceramic sealing of dense perovskite membranes were studied by making diffusion couples. Pure $LaCoO_3$ was found to be kinetically more stable to calcium silicate than Ca and Sr substituted $LaCoO_3$. In addition, the stability of the membrane / sealant interface was observed to be quite sensitive to the O/Si ratio of the calcium silicate. A suitable calcium silicate sealing material is a two-phase material with O/Si$\lesssim$4, having good sealing properties and moderate reactivity to the dense membrane material.

In paper VI we have studied the mechanical aspects of sealing dense ceramic membranes. Residual stresses in oxygen permeable membrane systems have been calculated by using a model based on the force balance approach for general asymmetric composites. The difference in thermal expansion coefficient (TEC) and the glass transition temperature of the sealant are the most significant quantities for establishing a residual stress state. The maximum permitted difference in TEC between membrane and support to keep the membrane stress below 100 MPa is $\sim 10^{-6}K^{-1}$, assuming no relaxation of the stress and separate sealing of the membrane. The critical part of the process is cooling the sealed membrane to room temperature due to long relaxation times of the residual stress in the membrane. Thus, the theoretical calculations predict that *in situ* sealing of the membrane to the support is necessary.

Preface

This work has been carried out at the Department of Chemistry, Norwegian University of Science and Technology (NTNU), in the period February 1996 - October 2000, including one year (September 1999 - July 2000) of maternity leave. The scientific work is presented in the form of six papers, out of which five have been / will be published in international journals. Paper VI appears only in this thesis. A list of the scientific papers is given after the contents. Two papers, VII and VIII, are included in the appendices. These served as a basis for the work on ceramic fuel cells (Papers II-IV). My contribution is mainly connected to paper VII where I have performed the major part of the experimental work during the first 6 months of my stay at the Department of Chemistry.

I want to express my sincere gratitude to my main supervisor Professor Mari-Ann Einarsrud for her interest and guidance of this work. Her knowledge and experience from materials science and related experimental methods have been of invaluable importance for my work. I also want to express my gratitude to Professor Tor Grande, who has been an important co-supervisor throughout these years. His interest and new ideas to my work have been a source of great motivation. In addition, he has contributed significantly to the discussion on phase-equilibria in paper V. I would also like to thank my co-supervisors Professor Ragnvald Høier and Associate Professor Kjell Wiik for assistance with experimental work and interpretation of results. Special thanks also to Dr. Kristin Breder who introduced me to the mechanical stability of interfaces.

I am grateful to the Norwegian scientific foundation VISTA for their financial support. Thanks also to the Research Council of Norway for their financial support during my stay at Siemens AG in Munich, Germany, September - December 1998.

I want to thank the staff at Department of Chemistry, especially my colleagues in block II, for making my stay at NTNU so enjoyable.

Finally, I give special thanks to my husband, Joakim, and my 1 year old daughter, Frida, for unending support and inspiration. The encouragement and interest from my parents and grandparents have also been most valuable to me.

Trondheim, October 2000
Sonia Faaland

Contents

List of scientific papers

Paper I S. Faaland, K.D. Knudsen, M.-A. Einarsrud, L. Rørmark, R. Høier, T. Grande: Structure, Stoichiometry, and Phase Purity of Calcium Substituted Lanthanum Manganite Powders, *J. Solid State Chem.*, **140**, 320 (1998).

Paper II S. Faaland, M.-A. Einarsrud, K. Wiik, R. Høier, T. Grande: Reaction between $La_{1-x}Ca_xMnO_3$ and CaO-stabilized ZrO_2, Part I: powder mixtures, *J. Mat. Sci.*, **34**, 957 (1999).

Paper III S. Faaland, M.-A. Einarsrud, K. Wiik, R. Høier, T. Grande: Reaction between $La_{1-x}Ca_xMnO_3$ and CaO-stabilized ZrO_2, Part II: Diffusion Couples, *J. Mat. Sci.*, **34**, 5811 (1999).

Paper IV S. Faaland, M.-A. Einarsrud, R. Høier: Reaction between $La_{1-x}Ca_xMnO_3$ (x=0.3 and 0.6) and CaO-stabilized ZrO_2 powder mixtures studied on a nano-meter scale, *J. Mat. Sci. Lett.*, **19** [15], 1379 (2000).

Paper V S. Faaland, M.-A. Einarsrud, T. Grande: Reactions between calcium and strontium substituted cobaltite ceramic membranes and calcium silicate sealing materials, *Chem. of Mat.*, In print.

Paper VI S. Faaland: Mechanical aspects of sealing dense oxygen permeable membranes, Only to appear in this thesis.

Additional papers (Appendices A and B):

Paper VII K. Wiik, C.R. Schmidt, S. Faaland, S. Shamsili, M.-A. Einarsrud, T. Grande: Reactions between Strontium-Substituted Lanthanum Manganite and Yttria-Stabilized Zirconia: I, Powder Samples, *J. Am. Ceram. Soc.*, **82** [3], 721 (1999).

Paper VIII K. Kleveland, M.-A. Einarsrud, C.R. Schmidt, S. Shamsili, S. Faaland, K. Wiik, T. Grande: Reactions between Strontium-Substituted Lanthanum Manganite and Yttria-Stabilized Zirconia: II, Diffusion Couples, *J. Am. Ceram. Soc.*, **82** [3], 729 (1999).

List of acronyms

SOFC Solid Oxide Fuel Cell

SEM Scanning Electron Microscopy

BSE Back Scattered Electron

TEM Transmission Electron Microscopy

STEM Scanning Transmission Electron Microscopy

HRTEM High Resolution Transmission Electron Microscopy

XRD X-Ray Diffraction

ESI Electron Spectroscopic Imaging

EDS Energy Dispersive Spectroscopy

GIF Gatan Imaging Filter

FEG Field Emission Gun

IR Infra Red

LM $LaMnO_3$

LSM $La_{1-x}Sr_xMnO_3$

LCM $La_{1-x}Ca_xMnO_3$

LCC $La_{1-x}Ca_xCoO_3$

LSC $La_{1-x}Sr_xCoO_3$

LMC $La_{1-x}M_xCoO_3$ (M=Ca or Sr)

CSZ $ZrO_2(CaO)$

YSZ $ZrO_2(Y_2O_3)$

LZ $La_2Zr_2O_7$

CZ $CaZrO_3$

SZ $SrZrO_3$

LO La_2O_3

1 Introduction

1.1 Upgrading of Natural Gas

The increasing demand for electrical energy and easily transportable fuels, combined with requirements of low emission of CO_2, has lead to an extensive international interest in upgrading of natural gas to value-added products. Fuel cells generate electricity from natural gas (or H_2) and are superior to other fossile energy conversion technologies with regard to energy efficiency and emission of pollutants [1]. Solid oxide fuel cells can convert natural gas directly to electricity, eliminating the need for an expensive external reformer system. The Norwegian interest in fuel cell technology is mainly due to:

- large natural gas reserves
- extensive high-power industry
- sparsely populated areas

Although natural gas reserves already exceed ever-diminishing oil reserves, only a small fraction of natural gas is being used as feed stock in the petrochemical industries. During the past several years, extensive efforts have focused on converting methane, the most abundant component of natural gas, to value-added products (such as easily transportable liquid fuels). In the conventional route for converting methane to methanol, syngas ($CO + H_2$) is produced in a first stage. Although direct partial oxidation of methane to form syngas with air as the oxygen source is possible, downstream processing requirements often can not tolerate nitrogen, and, therefore, pure oxygen is required. Thus, the most significant cost associated with partial oxidation is that of the oxygen plant. Oxygen-permeable membrane systems can be used for a low-cost direct conversion of methane to syngas at efficiencies >99% [2], without emission of nitric oxides. Such a system will operate without an externally applied electrical potential.

1.2 Solid Oxide Fuel Cells (SOFCs)

SOFCs essentially consist of two porous electrodes separated by a dense, oxygen-ion-conducting electrolyte. A schematic diagram of fuel cell operation is given in Figure 1. Oxygen supplied at the cathode (air electrode)

reacts with incoming electrons from the external circuit to form oxygen ions, which migrate to the anode (fuel electrode) through the oxygen-ion conducting electrolyte. At the anode, oxygen ions combine with H_2 (and/or CO) in the fuel to form H_2O (and/or CO_2), liberating electrons. Electrons flow from the anode through the external circuit to the cathode.

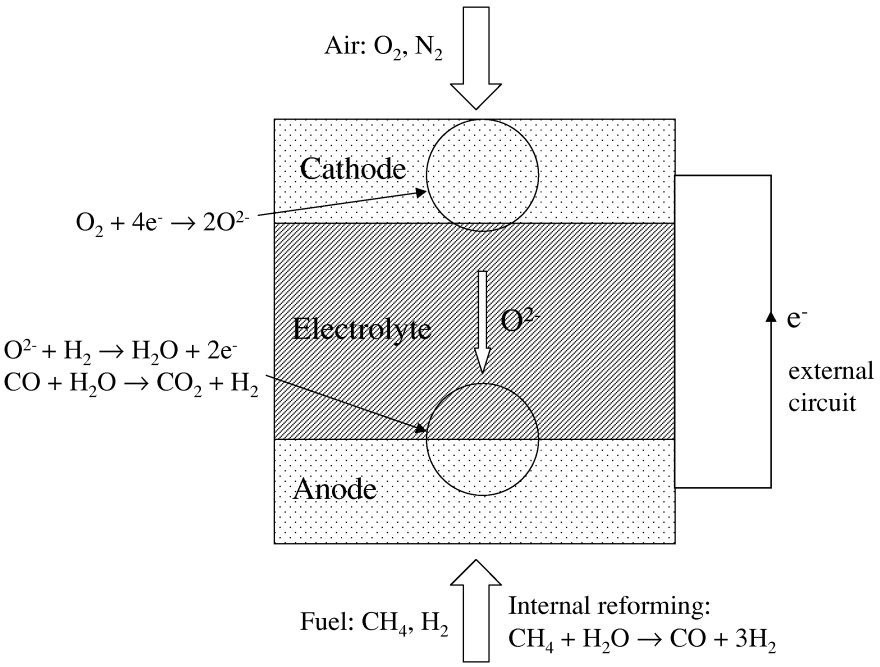

Figure 1: SOFC operational principle.

SOFCs of several different designs have been investigated; these include planar, monolithic and tubular geometries [3, 4]. The materials for cell components in these different designs are the same or very similar in nature. However, the designs differ in the extent of dissipative losses within the cells, in the manner of sealing between fuel and oxidant channels, and in making cell-to-cell electrical connections in a stack of cells (interconnect geometry).

Stabilized zirconia (ZrO_2), especially yttria-stabilized zirconia (YSZ), is the conventional electrolyte in SOFCs because the material possesses an adequate level of oxygen-ion conductivity at temperatures around 1000°C and exhibits desirable stability in both oxidizing and reducing atmospheres. The properties of stabilized zirconia have been extensively studied [5–7]. Because of the high operating temperature (1000°C) of the YSZ-based SOFC,

only noble metals or electronic conducting oxides can be used as cathode materials. Noble metals, such as platinum, palladium or silver are unsuitable for practical applications because of prohibitive cost (and insufficient long-term stability due to vaporization of silver). Several doped oxides and mixed oxides have been proposed and investigated [8,9]. The disadvantages of most of these materials are thermal expansion mismatch, incompatibility with the electrolyte and poor conductivity. Lanthanum manganite-based oxides, e.g. $La_{1-x}Ca_xMnO_3$ (LCM) and $La_{1-x}Sr_xMnO_3$ (LSM), are promising materials as cathodes because of their high electrical conductivity and relatively good compatibility with YSZ. Because of the reducing conditions of the fuel gas, metals can be used as SOFC anode materials. Nickel is most commonly used because of its low cost. To maintain the porous structure and to provide a thermal expansion coefficient acceptably close to those of the other cell components, nickel metal is often dispersed on the surface of a YSZ support (nickel/YSZ cermet).

If a SOFC is driven by natural gas, the high operating temperature (1000°C) will lead to carbon deposits. To increase the oxygen-ion conductivity at lower temperatures, YSZ-membranes much thinner than the standard 150 μm membranes can be made. A 5 μm YSZ membrane has recently been found to have an adequate oxygen ion conductivity at 600°C [10]. The benefit of the lower operating temperature is in addition to a reduction in carbon crude build-up, a lower heat stress on the apparatus itself. Other oxygen materials such as rare-earth-doped ceria, rare-earth-doped bismuth oxide and doped lanthanum gallates have been investigated as alternative electrolytes for SOFC [11–13]. But until recently, YSZ has been the most successfully employed due to high stability and good compatibility with the other cell components. However, the samarium-doped cerium oxide membrane is a far better oxygen-ion conductor than the standard YSZ electrolyte for temperatures below the conventional operating temperature of a SOFC (1000°C) [14, 15]. Thus, in the most recent approach in SOFC development, cerium dioxide is used as electrolyte [16]. Other designs are also coming up. Hibino et al. [16] describe a unique fuel cell design operating at temperatures below 500°C in which the hydrocarbons and air are pumped into a single chamber, where they surround the electrodes and electrolyte membrane. One side of the membrane is dabbed with nickel and serves as the anode, while $Sm_{0.5}Sr_{0.5}CoO_3$ on the other side serves as the cathode.

The principal components of a ceramic fuel cell stack are the electrolyte, the anode, the cathode and the interconnect. Each component serves sev-

eral functions in the fuel cell and must meet certain requirements. Each component must have the proper stability (chemical and mechanical) in oxidizing and/or reducing environments, chemical compatibility with other components and proper conductivity. The components for ceramic fuel cells must, in addition, have the similar coefficients of thermal expansion to avoid delamination or cracking during fabrication and operation. Last but not least, the components of a ceramic fuel cell must be compatible not only at the operating temperature but also at the higher temperatures at which the ceramic structures are fabricated. During fabrication and operation, secondary phases tend to form at the cathode-electrolyte interface, causing reduced stability and efficiency of the SOFC.

1.3 Dense Oxygen Permeable Membranes

Dense ceramic membranes with mixed oxygen ionic and electronic conductivity are receiving considerable attention due to their possible application for oxygen separation and partial oxidation of natural gas [17–21]. Oxygen permeable membrane systems consist of ceramic membranes sealed to a support material (Fig. 2). Air flows on the outside of the membrane and methane flows through the inside. No external electrodes are required, and if the driving potential of transport (ΔpO_2) is sufficient, the partial oxidation reactions should be spontaneous. The oxygen permeation fluxes can be improved when using thin film membranes deposited onto a porous substrate [22]. Ceramic membranes can be shaped into a hollow-tube reactor (Fig. 2). Honeycomb, corrugated or disk reactors are also possible. However, regardless of which membrane design is chosen, a gas-tight seal between membrane and support is essential.

Perovskite-related oxides represent one of the most promising groups of the mixed-conducting membrane materials due to suitable transport properties and stability in different atmospheres [20, 21, 23–26]. A- and B-site substituted perovskites in the La-M-Fe-Co-O (M=Sr,Ba,Ca) system, i.e. $La_{1-x}M_xCo_{1-y}Fe_yO_{3-\delta}$, exhibit high oxygen permeation fluxes and appreciable electronic conductivity at ~800°C [27–31] and are, thus, candidate materials for dense oxygen permeable membranes.

Due to the high degree of commercial interest, the issue of sealing is rarely discussed in great detail in the literature. However, various glass-based materials, largely based on SiO_2, for SOFC sealing purposes have been reported. The sealing materials mentioned in the literature can be divided

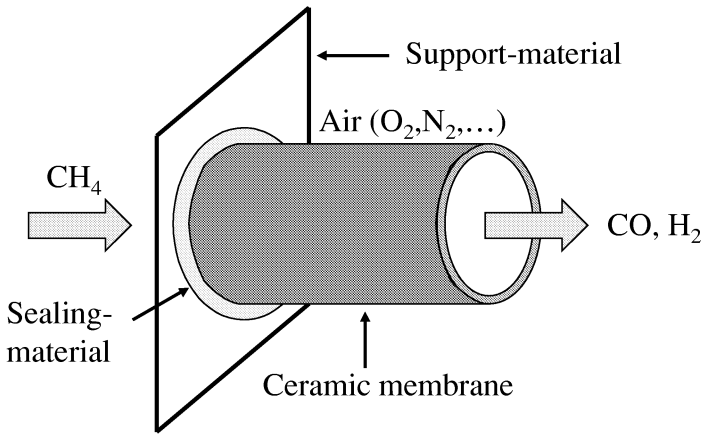

Figure 2: Schematic drawing of an oxygen permeable membrane system used for direct conversion of methane to syngas (CO + H_2).

into the following compositional groups: alkali silicate glasses, mica glass ceramics, alkali earth borosilicate glasses and alkali earth aluminosilicate glasses.

Dense oxygen permeable membranes can have immense impact on the natural-gas industry. However, there is still a need for further research on the fundamentals of membrane preparation, the effects of material properties on transport mechanism and the long-term thermal and chemical stability of the membrane and the membrane / sealant interface. During the sealing process and operation, the sealing materials tend to react with the ceramic membranes to form secondary phases. The chemical reactions involved in bonding cannot be generalized, but must be determined in each individual case. Moreover, the rate-controlling mechanisms for formation of reaction layers are not yet fully understood, which means that further work is required.

1.4 Aim of the Present Work

The aim for this work is to gain fundamental understanding of the stability of ceramic interfaces in general, and more specifically to heterophase solid state interfaces related to solid oxide fuel cells and dense oxygen permeable

membranes. The stability of such interfaces can be reduced due to interdiffusion of ions and formation of secondary phases. In this thesis reaction mechanisms are discussed and requirements and properties of suitable materials for use in solid oxide fuel cells and oxygen permeable membrane systems are determined.

Perovskite-based materials are potential candidates for SOFC cathodes and interconnects and oxygen permeable membranes. Over the last years, there have been various suggestions regarding the crystal structure of $La_{1-x}Ca_x MnO_3$ (LCM), a promising cathode material. The aim of paper I was therefore to study the structure and stoichiometry of this compound.

The reactivity of LCM with yttria stabilized zirconia (YSZ) has been studied by several researchers [32–35]. However, the reactivity of LCM with other electrolyte materials has not been examined thoroughly. The aim of papers II, III and IV was to study a model system for the electrode / electrolyte interface consisting of LCM and calcia stabilized zirconia (CSZ). The thermodynamic driving force for the formation of secondary phases is reduced in this system by replacing yttria in the zirconia with calcia. This substitution was performed in order to obtain a better understanding of the effect of different dopants on the stability of the electrode/electrolyte materials conventionally used in SOFC (LSM and YSZ) [36–39].

Although recent reports have described various perovskite-type materials that could be used in ceramic membrane reactors, little work appears to have focused on the problems associated with chemical stability of the materials under operating conditions and with the mechanical problems of sealing the membrane material. The aim of paper V was to study a model system for the membrane / sealant interface consisting of $La_{1-x}M_xCoO_3$ (M=Ca, Sr; x=0, 0.2, 0.5) (LMC) and calcium silicate ($CaSiO_3$ / Ca_2SiO_4). Potential industrial membranes are supposed to contain La_2O_3, CaO and SrO as the more basic oxide constituents and Co as one among two or more transition elements [2, 40]. Likewise, Ca-silicates are considered as potential components for industrial sealants. For oxygen permeable membrane systems, residual stresses are developed in membrane, sealant and support during preparation and operation. The aim of Paper VI was to perform a calculation of the permanent stresses at interfaces in dense oxygen permeable membrane systems and to identify important parameters determining possibility for failure.

2 Review of Previous Work

2.1 Perovskite Materials

Perovskites have the general formula ABO_3, where A is a large cation, usually a rare earth metal, an alkali metal or an alkali earth metal and B is a smaller cation, often a transition metal. The highest temperature perovskite phase usually has the ideal, cubic structure. In this structure A-site cations coordinate with 12 anions: 4 O(1) and 8 O(2) ions [1]. B-site cations coordinate with 6 anions: 2 O(1) and 4 O(2) ions. When the cations are displaced or the octahedra, BO_6, are tilted or rotated, different types of structures are produced. These structures are always of lower symmetry than cubic, giving rise to larger unit cells [41]. Goldschmidt found that the perovskite structure distorts to tetragonal, rhombohedral or orthorhombic symmetry when $\sim 0.75 < t < 1$, where $t = (R_A + R_O)/\sqrt{2(R_B + R_O)}$ [42]. R_X denotes the ionic radius of X. In these lower symmetry structures, the coordination numbers of the cations are reduced compared to the ideal, cubic perovskite structure.

$LaMnO_{3+\delta}$ is a perovskite that crystallizes with rhombohedral symmetry, space group $R\bar{3}c$ [43,44]. $SrMnO_3$, however, has a non-perovskite hexagonal unit cell [45,46]. The solid solution limit of strontium in $La_{1-x}Sr_xMnO_{3\pm\delta}$ is x=0.7 [44]. For application in SOFC, compositions up to x=0.5 are considered. The behaviour of the solid solution series $La_{1-x}Sr_xMnO_3$ is dominated by the end member $LaMnO_{3\pm\delta}$. The structure of $La_{1-x}Ca_xMnO_3$, however, is dominated by $CaMnO_3$, which has an orthorhombic perovskite structure (Pnma) [47], similar to the structure of stoichiometric $LaMnO_{3.00}$ [48]. Over the last years there have been various suggestions regarding the symmetry of the $La_{1-x}Ca_xMnO_3$ compounds. However, a recent study by Radaelli et al. [49] concludes that the structure is orthorhombic with space group Pnma for x=0.25 and x=0.50 in the temperature range 0-350 K.

$LaCoO_3$ has a rhombohedral crystal structure ($R\bar{3}c$) at room temperature [50]. When La is substituted by Sr (or Ca) at room temperature the rhombohedral angle decreases linearly with increasing Sr content (x), and the structure becomes cubic at x=0.55 [51]. $SrCoO_x$ has two perovskite-like crystallographic forms: brownmillerite and 2H-related hexagonal perovskite, the existence of which depends on the spin configuration of cobalt. $CaCoO_x$ does not exist [52].

[1] O(1) and O(2) have different crystallographic positions, respectively 4(c) and 8(d).

Non-stoichiometry in perovskite oxides arises from cation deficiency (in A or B site), oxygen deficiency or oxygen excess. Oxygen non-stoichiometry in perovskite oxides is more common than that involving vacancies in the cation sublattice. The oxygen non-stoichiometry is indicated by δ in $ABO_{3\pm\delta}$. Oxygen deficiency is by far the most common non-stoichiometry, but oxygen excess perovskites like $LaMnO_{3.16}$ are also known. High concentrations of oxygen vacancies can be induced into the $ABO_{3\pm\delta}$ structure by the substitution of lower valent cations onto either the A- or B-sites, e.g. $A_{1-x}A'_xB_{1-y}B'_yO_{3\pm\delta}$. The oxygen content decreases with increasing values of x or y because the sum of valences of the cations determines the oxygen stoichiometry. Low oxygen activity causes a higher oxygen deficiency. In addition, the oxygen content decreases with increasing temperature at constant oxygen activity. Kuo et al. [53, 54] have shown that the oxygen vacancy content of $LaMnO_{3\pm\delta}$ is small, even at sufficiently low oxygen activity. $LaCoO_{3-\delta}$, however, shows a large oxygen deficiency at high temperature [55,56]. Defect ordering in oxygen deficient perovskites involves a conservative mechanism in the sense that the vacancies are assimilated into the structure, resulting in large supercells of the basic perovskite structure. The type of superstructure formed depends, however, on the identity of the B-cation[2]. Ionic conductivity is closely related to the ordering of oxygen vacancies in the perovskite structure [57].

Perovskite materials possess a wide specter of electrical and magnetic properties. Magnetic properties will not be discussed here. Perovskites may be electrically insulating, semi-conducting or metallic. Perovskite type oxides with trivalent transition metal ions in the B and a trivalent rare earth in the A-position, such as $LaMnO_{3+\delta}$ and $LaCoO_{3-\delta}$, have p-type intrinsic conductivity. $LaCoO_{3-\delta}$ has a higher electrical conductivity than $LaMnO_{3+\delta}$ under similar conditions [58, 59]. The electrical conductivity is enhanced by substituting a lower-valence cation on either the A- or B-sites, e.g. $La_{1-x}Sr_xMnO_{3\pm\delta}$ and $La_{1-x}Sr_xCoO_{3-\delta}$. $La_{1-x}Sr_xMnO_{3\pm\delta}$ shows a semi-conducting to metallic transition at x$\sim$0.5 [60]. A similar transition is observed in $La_{1-x}Sr_xCoO_{3-\delta}$ for x$\sim$0.25 [51]. The electronic conductivity takes place via the small polaron conduction mechanism in both cases.

Perovskite materials possessing both electronic and ionic conductivity are called mixed conductors. Both $LaMnO_{3\pm\delta}$ and $LaCoO_{3-\delta}$ are mixed conductors, and the conductivity increases by substituting lower valent cations at A- or B-site. Mixed conductivity is a requirement for dense oxygen per-

[2]Superstructures may also arise due to ordering of cations or cation vacancies.

meable membranes. A- and B-site substituted perovskites in the La-M-Fe-Co-O (M=Sr,Ba,Ca) system, i.e. $La_{1-x}M_xCo_{1-y}Fe_yO_{3-\delta}$, represent one of the most promising groups of the mixed-conducting membrane materials [27–31].

2.2 Chemical Kinetics of Phase Boundaries in Solids

The stability of interfaces formed between inorganic materials is of great technological importance. Interdiffusion and chemical reactions at the interface affect the properties and performance of multi-phase systems. The chemical reaction at the interface is governed by the thermodynamics and reaction kinetics of the system under consideration. The former determines which phases are stable at the processing and operating conditions and the latter determines how much of a phase is formed. In addition, kinetics is relevant for non-equilibrium systems. If the thermodynamics and mobilities of all elements in all phases are known, the sequence, morphology and thickness of newly formed phases can be predicted to a large extent. However, often no or only incomplete thermodynamic and diffusion data are available. In addition, there may be problems in understanding the interrelations between the defect structure of materials, nucleation of new phases, mechanical stresses and morphological evolution of the reaction zone.

The general mechanism of solid-solid reactions consists of initial formation of one or more solid products that spatially separate the reactants. Subsequent reaction requires mass transport through product-layers. If we assume that thermodynamic equilibrium is attained at the interface and that diffusion is the rate-limiting step, the kinetics of the reaction layer formation in the reaction zone follows a parabolic law

$$\Delta\xi_p(t) = \sqrt{2k_p t}, \tag{1}$$

where $\Delta\xi_p$ is the increase in layer thickness, k_p is a transport coefficient related to solid state diffusion and t is time [61]. In pseudo-binary systems more than one product phase may form between the reactants. The more interfaces separating the different product phases, the more likely it is that deviations from local equilibrium occur. Local equilibrium versus non-equilibrium at interfaces in the $LaCoO_3$ / ZrO_2 system during reaction is shown in Fig. 3. If, however, we assume that local equilibrium is established during reaction, each individual phase in the reaction layer grows parabolically according to Eq. 1. Adding the different $\Delta\xi_p$'s together, one

obtains the total thickness

$$\Delta\xi(t) = \sqrt{2kt}, \qquad \sqrt{k} = \sum_{p=1}^{n} \sqrt{k_p}. \tag{2}$$

If, however, local equilibrium is not established, the phases which exist in equilibrium may not all form. This is sometimes observed in early stages of a reaction. Also, nucleation barriers can inhibit the formation of some phases in a multi-phase reaction layer [61].

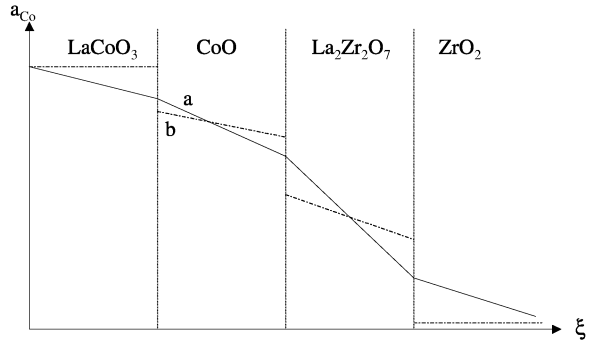

Figure 3: Co activity vs. location for the $LaCoO_3$ / ZrO_2 system during reaction. (a) Local equilibrium is established. (b) At interfaces local equilibrium is not established. (Based on a figure by Schmalzried [61]).

Ultra thin reaction layers grow without creating any noticeable stress in the bulk of the reactants. However, increasing reaction layer thickness introduces stress energy which, due to the change of both the driving force and component mobilities in the reaction layer, influences the kinetics of product layer formation. Schmalzried [61] has shown that the driving force for reaction is proportional to $\Delta\xi^{-1}$, again leading to a parabolic rate law. However, if the evolving stress energy contained in the reactants is also taken into account, the overall stress energy depends on the thickness of the reaction layer, which invalidates the parabolic growth and slows down the reaction rate. In principle, this can stop the reaction.

In solid state reactions between ionic solids (oxides), the fluxes due to differently charged ions must be coupled during the reaction to maintain electrical neutrality. In the classical mechanism suggested by Wagner [62, 63] electro-neutrality is maintained by counter diffusion of cations through the product layer. Consequently, the slower moving cation essentially determines the rate of reaction and at which interface the product layer grows. Another reaction mechanism involves simultaneous diffusion of cations and

anions across the product layer. An example is the simultaneous diffusion of Me^{2+} and O^{2-} across the orthosilicate phase, Me_2SiO_4, in a MeO - SiO_2 / $MeSiO_3$ diffusion couple [61]. Thus, when Si^{4+} is the slowest moving ion, the orthosilicate should form at the Me_2SiO_4 / SiO_2 ($MeSiO_3$) interface. Unfortunately, the understanding of the solid state kinetics in orthosilicates is unsatisfactory for other silicates with interlinked tetrahedra.

2.3 Cathode - Electrolyte Interface Reactions in SOFCs

Solid oxide fuel cells (SOFC) and ceramic oxygen-permeating membranes are examples of systems possessing solid state interfaces between a perovskite type oxide (ABO_3) and another ceramic material. The reactivity of LCM / LSM with yttria stabilized zirconia (YSZ) has been studied by several researchers [32–38, 64]. A number of these investigations have shown that the formation of secondary phases are dependent on the dopant level in the perovskite. A short review is offered by Minh [64]. The formation of secondary phases such as $La_2Zr_2O_7$(LZ) and $SrZrO_3$(SZ) / $CaZrO_3$(CZ) at the interface, as well as inter-diffusion of cations between the cell components, having a negative impact on the SOFC performance, have been observed.

A reaction mechanism has been proposed by Taimatsu et al. [35] for the formation of LZ at the $La_{1-x}Ca_xMnO_3$ (x=0, 0.1, 0.2)/YSZ boundary. A layer of $La_2Zr_2O_7$ is formed at the $La_{1-x}Ca_xMnO_3$ / YSZ interface after an induction period, and the formation is accelerated when the $La_{1-x}Ca_xMnO_3$ phase is porous. The reaction proceeds by unidirectional diffusion of La, Mn and/or Ca ions, mainly Mn ions, into YSZ.

Yokokawa et al. have made a series of thermodynamic analyses on the chemical stability of perovskite oxides and fluorite-type oxide solutions related to high-temperature solid oxide fuel cells [65–71]. Thermodynamic stabilities of interfaces between perovskite oxides and cubic stabilized zirconia have been analyzed by chemical equilibria calculations and construction of chemical potential diagrams [72–74]. Calculation results revealed that the reactivity of $(La_{1-x}A_x)_yMnO_{3\pm\delta}$ (A=Ca,Sr) can be divided into two categories in terms of the A-site occupancy, y. When the A-site occupancy is close to unity, the formation of LZ or SZ occurs at the manganite - YSZ interface, while no zirconate is formed when the A-site occupancy is small; however, the manganese dissolution into YSZ becomes significant [73]. Thermodynamic calculations by Yokokawa et al. [74] have demonstrated that

$La_yMnO_{3\pm\delta}$ may coexist with YSZ when the A-site occupancy is less than 0.86 (at 1300°C in air). In addition, it was proposed that a high oxygen potential was needed for the formation of LZ at the lanthanum manganite (LM)/YSZ interface according to the reaction:

$$La_yMnO_3(s) + (y - y')ZrO_2(s) + \frac{3(y-y')}{2}O_2(g) = La_{y'}MnO_3 + \frac{(y-y')}{2}La_2Zr_2O_7.$$

This reaction is not destructive. During reaction, y changes to a smaller value, and the driving force for the $La_2Zr_2O_7$ formation eventually ceases when y reaches the critical value, and perovskite, zirconia and LZ are equilibrated with each other.

Van Roosmalen et al. have contributed significantly to the understanding of defect chemistry, sintering behaviour and properties of lanthanum manganite [36, 75–79]. Van Roosmalen et al. [75] showed that the sinterability of LSM powders decreased with increasing strontium content of the LSM phase and increased when the ratio between La and Mn was below unity. Evju [80] and Watterud [81] also confirmed that A-site deficient manganites sintered at lower temperatures compared to stoichiometric materials. Thus, the La:Mn ratio is a significant parameter for the performance of $LaMnO_{3\pm\delta}$ as cathode material in SOFCs. In addition to a lower sintering temperature, a La:Mn ratio smaller than unity causes an increased electrical conductivity [82], an increased inertness towards the electrolyte material (YSZ) [83] and a decreased thermal expansion coefficient, i.e. an improved compatibility with the other SOFC components [83]. The effects of A-site deficiency are probably related to an increased $[Mn^{4+}]/[Mn^{3+}]$ ratio and/or an increase of oxygen vacancy concentration, required for charge compensation [83]. Clearly, the dopant level of Sr in LSM as well as the ratio between A-site and B-site cations in the perovskite are expected to affect the thermodynamics and kinetics of the electrolyte / cathode interface in SOFCs.

2.4 Chemical Aspects of Sealing Ceramic Materials

Glass-Based Sealing Materials

Glasses are the most commonly used sealants. Softening points and thermal expansion coefficients are highly variable from glass to glass. The thermal property that unifies all glass compositions and serves as the basis for the definition of glass is viscosity. Under the action of applied stress, a viscous material will flow. The lower the viscosity, the higher the flow rate. The

viscosity, η, of a glass is well described by an equation of the Vogel-Fulcher form

$$\eta = \eta_0 \cdot \exp\left(\frac{A}{T - T_0}\right), \tag{3}$$

where A, T_0 nd η_0 are material constants and T is absolute temperature. Of importance to the build-up of residual stress in glasses are the softening and glass transition temperatures, T_s and T_g. The viscosities associated with these temperatures for all glasses are, respectively, $10^{7.6}$ P and 10^{13} P [84].

At the sealing temperature the sealant must have a suitable viscosity allowing deformation, i.e. a viscosity close to the softening point such that a gas-tight seal can be formed. At the operating temperature, however, the viscosity should be higher to withstand a gas overpressure. As the temperature is lowered, a point will be reached (T_g) where stress relaxation of the glass becomes so slow that any differences in thermal contraction between the two materials can no longer be accommodated. A further decrease in temperature will then result in the creation, within the timescales involved, of residual stress. Thus, a suitable operating temperature is just above T_g. Stress introduced during sealing or operation by thermal gradients or differences in thermal expansion coefficient (TEC) may then be relaxed at the operating temperature, preventing formation and growth of cracks. However, strong bonding puts some restriction to the TEC matching between the components, since stresses may be accumulated below T_g, where the glass is rigid. Unlike most crystalline materials, glasses do not have fixed stoichiometry. Modifications of relative component concentrations are therefore permitted within certain limits, which enables continuous changes of glass properties, e.g. TEC.

Glass-ceramics offer a number of engineering advantages over glasses. Primarily, glass-ceramics can be easily shaped and formed while still in the molten state, and following controlled nucleation and crystallization, they exhibit properties closely approaching those of ceramics. Thermal properties of glass-ceramics can be tailored in a wide range, permitting close expansion match to numerous materials. As a result, for hermetic seal applications, the advantages of using glass-ceramics are clear. Ideally, interfacial reactions and bonding between the glass precursor and the ceramic occur during an initial high-temperature stage of the sealing process. Further heat treatment allows subsequent crystallization to proceed, yielding a glass/polycrystalline composite microstructure with greater strength and toughness, and often more suitable thermal expansion compatibility with

the other material being sealed.

Chemical Bonding

The main requirements for the formation of a high-quality seal or coating are the ability to form a strong chemical bond between the components and the ability to match as closely as possible the thermal expansion characteristics of the other materials. Chemical bonding is achieved at interfaces by [85]:

1. Formation of an intimate, atomic contact interface
2. Reaction to reach thermodynamic equilibrium at the interface

The second step is the most critical. In practically all cases thermodynamic equilibrium is achieved by interface reactions. The simplest reaction is the solution of one phase in the other to form an immediate equilibrium saturation at the interface. A continuation of the reaction is associated with diffusion into the bulk. Hence, the overall reaction is referred to as diffusion bonding. Compound formation may also take place in order to reach equilibrium, but formation of undesirable reaction products that may alter the properties at the interface must be prohibited. In oxide systems, the formation of new oxide compounds is depending on the acid / base properties of the oxide constituents of the primary phases. A selection of acidity parameters for different oxides is given in Table 1 [3].

Table 1: Selection of acidity parameters, a, for different oxides (from [86]).

	SiO_2	ZrO_2	CoO	MnO	La_2O_3	Y_2O_3	CaO	SrO	BaO
a	0.9	0.1	-3.8	-4.8	-6.1	-6.5	-7.5	-9.4	-10.8

It is generally agreed among SOFC and oxygen permeable membrane developers that one of the main challenges encountered is to obtain long term stable operational seals. But due to the high degree of commercial interest, the issue of sealing is rarely discussed in the open literature. However, a few studies have been reported, and silica based materials are usually considered as potential sealing materials [87–92].

[3] The acidity scale is defined by Schmidt [86].

Interdiffusion of cations at sealant - SOFC component interfaces has been investigated [87–90]. In a study on interface reaction between Pyrex glass (81 wt% SiO_2, 13 wt% B_2O_3, 4 wt% Na_2O, 2 wt% Al_2O_3) and electrolyte (YSZ) Horita et al. [88] reported three zones at the interface vicinity: (1) the glass phase in which some components in the perovskite phase dissolved, (2) reaction zone, and (3) the perovskite phase from which some components migrated. Basic oxides such as CaO and Y_2O_3 easily diffused from the electrolyte to Pyrex glass because of their affinities of silicon. Silicon, however, did not dissolve into the perovskite phase but reacted with La- and Ca-components to form La- and Ca-silicates in the reaction zone.

In a study on the chemical stability of phosphate glass / interconnect interfaces in SOFC environment, Larsen and James [89] never found diffusion of glass components into the bulk of the interconnect material ($La_{0.8}Ca_{0.22}CrO_3$) despite strong interface reaction. However, Ca-diffusion was found up to 1 mm inside the glass. A similar study on the influence of sealing material on nickel/YSZ anodes [90] revealed no presence of Si in the anode material after heating at 1000°C.

Horita et al. [91] found that it was inevitable to form reaction products between lanthanum chromite and silica-based glasses. Calcium lanthanum silicates ($Ca_2La_8(SiO_4)_6O_2$ and $Ca_3La_6(SiO_4)_6$) were the major reaction products in addition to chromium oxide (Cr_2O_3). The formation of the calcium silicates and lanthanum silicates in the reaction zone at 1200°C was found to cause a deficiency of A-site cation in the perovskite (ABO_3), eventually leading to the decomposition of the perovskite structure. A study on the compatibility of mica-glass ceramics and interconnect ($La_{0.8}Ca_{0.22}CrO_3$) by Yamamoto et al. [92] also revealed a reaction layer containing double silicates, e.g. $Ca_2La_8(SiO_4)_6O_2$.

2.5 Mechanical Problems of Oxygen Permeable Membranes

To avoid cracking and delamination, the membrane material should have a thermal expansion coefficient (TEC) matching that of the sealing and support materials. Reviews on TEC of alternative membrane, sealing and support materials are offered by Kharton et al. [93], Donald [94], Larsen and James [89] and Anderson [95].

The membrane must be sufficiently stable both in highly reducing (syngas side, $pO_2 \sim 10^{-16} - 10^{-19}$ atm) and highly oxidizing (air side, $pO_2 \sim 0.2$ atm) environment (Fig. 2). The overall expansion of an oxygen deficient material

contains two components: one that is caused by the temperature and one that is caused by the change of oxygen content (chemical expansion). The chemical expansion of $La_{0.6}Sr_{0.4}Co_{0.2}Fe_{0.8}O_{3-\delta}$ was investigated by Stevenson et al. [31] by isothermal dilatometry in the pO_2 range from 1 atm to 10^{-5} atm. The expansion is caused by the gradual reduction of tetravalent cations to larger trivalent (and even divalent) transition metal ions as the pO_2 decreases. An overall expansion [4] of a $La_{0.6}Sr_{0.4}Co_{0.2}Fe_{0.8}O_{3-\delta}$ membrane of approximately 0.35% due to the pO_2-gradient has recently been observed by Hendriksen et al. [96]. Hendriksen et al. [96] also found the maximum tensile stress in a $SrFeCo_{0.5}O_x$ membrane exposed to air and a pO_2 of 10^{-16} atm at either side at 1000°C to be 300 MPa, far higher than the fracture strength of the material. However, this material has been demonstrated capable of functioning as a syngas reactor for hundreds of hours [97]. Thus, some of the assumptions leading to the predictions of such high stresses must be erroneous, as stated by Hendriksen et al. [96].

Mechanical failures caused by insufficient dimensional stability of potential syngas membrane materials exposed to a pO_2-gradient have been reported. Pei et al. [98] observed two types of fractures occurring on the $Sr(Co,Fe)O_x$-type oxygen membrane reactors. The first type of fracture was the consequence of an oxygen gradient in the membrane. This causes a lattice mismatch inside the membrane, leading to fracture. The second type of fracture, however, was the result of a chemical decomposition. Laqua and Schmalzried [99,100] found an important phenomenon concerning high-temperature stability of ternary oxides, $A_nB_mO_x$: A ternary oxide may kinetically decompose when it is placed in an oxygen potential gradient, even though the oxygen potential is restricted within a stability region for the ternary oxide. Laqua and Schmalzried [99,100] attributed the driving force of kinetic decomposition to the difference in cation diffusivity in an oxygen potential gradient.

[4] The term overall expansion refers to the expansion that a free membrane would experience when exposed to the considered pO_2-gradient.

3 Summary and Discussion of the Work

This thesis consists of three parts: 1) Structure of Ca-substituted lanthanum manganite (Paper I), 2) Reactions between cathode and electrolyte for SOFC applications (Papers II-IV and Papers VII and VIII) and 3) Chemical and mechanical aspects of sealing dense oxygen permeable membranes (Papers V and VI). The main goal of the thesis is to get a fundamental understanding of phase boundaries in solids. In this section important results will be outlined, focusing on conclusions relating the different parts. For additional conclusions, I refer to the results in each paper.

In part 1 (Paper I) $La_{1-x}Ca_xMnO_3$ (LCM) has been extensively studied. The structure refinement revealed that $La_{1-x}Ca_xMnO_3$ with x=0.2, 0.3, 0.4 and 0.6 has orthorhombic symmetry with space group Pnma. A strong correlation was observed between the cooling rate from the calcination temperature and the powder quality, indicating the importance of a homogeneous oxygen stoichiometry.

In part 2 we have studied both the cathode/electrolyte materials conventionally being used in SOFC (LSM and YSZ) (Papers VII and VIII) and a model system consisting of LCM and calcia stabilized zirconia (CSZ) (Papers II-IV). The thermodynamic driving force for formation of secondary phases is reduced in this model system due to the replacement of yttria in zirconia with calcia. The main differences between the LCM/CSZ system and the LSM/YSZ system can be summarized as follows:

1. The semi-quantitative amounts of secondary phases are about 50% lower in the LCM/CSZ system compared to the LSM/YSZ system.

2. Equilibrium is established significantly faster in the LCM/CSZ system than in the LSM/YSZ system.

There are, however, also important similarities between the LCM/CSZ and LSM/YSZ systems:

1. The most chemically stable interface is observed when the lanthanum manganite contains 30 mole% dopant cations on La-site.

2. Porous microstructure and the observation of orthorhombic lanthanum manganite support the reductive nature of the reactions in the LCM/CSZ and LSM/YSZ systems.

The referred minimum in reactivity between lanthanum alkali earth manganite and cubic stabilized zirconia can be interpreted well in terms of phase relations and related thermodynamic properties [74]. At that particular composition, $La_{0.7}(Ca,Sr)_{0.3}MnO_3$, the perovskite can be in equilibrium with both $CaZrO_3$ / $SrZrO_3$ and $La_2Zr_2O_7$. This composition depends on the thermodynamic properties of the perovskite solid solution and of $CaZrO_3$ / $SrZrO_3$ and $La_2Zr_2O_7$. The reductive nature of the reaction between LCM/LSM and CSZ/YSZ is observed for all systems, except *pure* $LaMnO_3$/YSZ where the oxidative reaction proposed by Yokokawa et al. [74] is the dominating reaction. Based on results from both the LCM/CSZ and LSM/YSZ systems, it is proposed that A-site deficient lanthanum manganite and cubic stabilized zirconia are coexistent phases only when both phases are present in ample amounts due to considerable solid solubility between the two phases. Hence, we assume that a thin film of an electrode material on a zirconia substrate will always be unstable. An important point of the thermodynamic calculations by Yokokawa et al. [74] is that significantly A-site deficient lanthanum manganite should not react with ZrO_2. However, in these calculations, solid solubility is neglected.

In part 3, paper V, we have studied the chemical stability of $La_{1-x}(Ca,Sr)_x CoO_3$ (LMC) and $CaSiO_3/Ca_2SiO_4$ as simplified materials for the membrane and the sealing material in dense oxygen permeable membrane systems. The results reveal that minimum reactivity is obtained when there is no Ca or Sr substitution in the perovskite, i.e. x=0. Thus, there is a qualitative difference from the LCM/CSZ system, where minimum reactivity is obtained for a finite value of x ($\approx$0.3). However, the driving force for the reaction is an extraction of basic oxides from the perovskite in both systems. A comparison of the reaction mechanisms in the LCM/CSZ and LCC/$CaSiO_3$ diffusion couples is given in Table 2.

In the LCM/CSZ system the B-site element, Mn, is the most mobile cation due to the high solid solubility in CSZ [101]. B-site depletion in the perovskite causes exsolution of La_2O_3 for $x \leq 0.2$. Ca is observed to be removed from LCM for $x > 0.3$ because the acidity of ZrO_2 is high enough to make a reaction with the basic oxide CaO. SiO_2 is a much stronger acid than ZrO_2 [102], causing a total extraction of CaO from the perovskite phase in the LCC / $CaSiO_3$ system, giving rise to $LaCoO_3/CaSiO_3$ as the kinetically most stable interface. A-site depletion of the perovskite causes exsolution of CoO and eventually decomposition of the perovskite. However, the diffusion of the B-site element, Co, into $CaSiO_3$ is insignificant, in accordance with the CoO - SiO_2 - CaO phase diagram [103]. Thus, the most significant

Table 2: Comparison of the reaction mechanisms in the LCM/CSZ and LCC/$CaSiO_3$ diffusion couples.

LCM/CSZ	LCC/$CaSiO_3$
Diffusion of Mn into CSZ[†] (solid solution)	Insignificant diffusion of Co into $CaSiO_3$
Minor counter-diffusion of Zr	No counter-diffusion of Si
Reaction between CaO from LCM and CSZ for $x \geq 0.3$ Formation of CZ	Reaction between CaO from LCC and $CaSiO_3$ for $x \geq 0$ Formation of $Ca_3Si_2O_7$
Exsolution of La_2O_3 in LCM for $x \leq 0.2$	Exsolution of CoO in LCC
Reaction between La_2O_3 and CSZ[‡] Formation of LZ	Reaction between CaO and $Ca_2Si_2O_7$ Formation of Ca_2SiO_4
Diffusion of La/Ca through LZ and CZ $\Longrightarrow$ growth of CZ into CSZ and LZ into CZ/CSZ	Diffusion of Ca through Ca_2SiO_4 and $Ca_3Si_2O_7$ $\Longrightarrow$ growth of $Ca_3Si_2O_7$ into $CaSiO_3$ and Ca_2SiO_4 into $Ca_3Si_2O_7$
	Diffusion of La into Ca_2SiO_4 $\Longrightarrow$ formation of $Ca_aLa_b(SiO_4)_6$ for $x \leq 0.2$

[†]In LSM/YSZ diffusion couples Mn has been observed to diffuse into YSZ along grain boundaries (Paper VIII), while in the LCM/CSZ diffusion couples volume diffusion of Mn was observed (Paper III).

[‡]Eventually, diffusion of Zr^{4+} through the CZ-layer.

difference in reaction mechanism between the LCM/CSZ and LCC/$CaSiO_3$ systems is the diffusion of the B-site element of the perovskite. The significant diffusion of the B-site element (Mn) in the LCM/CSZ system is in accordance with observations in the LCM/YSZ system [35]. Despite of the difference in diffusion rate of the B-site element, the similarities in the reaction mechanisms for the LCM/CSZ and LCC/$CaSiO_3$ diffusion couples are obvious (Table 2).

A potential industrial sealing material for SOFC and dense oxygen permeable membranes is supposed to contain SiO_2 as an acidic oxide constituent and CaO as a basic constituent. In the two component system CaO-SiO_2 the mixing free energies of formation, ΔG_{mix}, for $CaSiO_3$ and Ca_2SiO_4 are respectively -58 kJ/mole and -62 kJ/mole [104]. Thus, a driving force for the LMC/$CaSiO_3$ reaction is the formation of orthosilicate from metasilicate. The observed decomposition of $CaSiO_3$ indicates that the activity of SiO_2 is too high to allow it to coexist with LMC. Ca_2SiO_4, on the other hand, has a lower SiO_2 activity allowing it to coexist with the perovskite. Based on the consideration of the SiO_2-activity in the CaO-SiO_2 system, it is obvious that the O/Si ratio is an excellent indicator of the thermodynamic stability of calcium silicates against LMC. We recommend to use a two-phase glass-ceramic sealing material consisting of orthosilicate with small amounts of metasilicate or disilicate glass. The glass is included to promote adequate sealing properties.

In paper V, $LaCoO_3$ was found to be kinetically more stable to calcium silicate than Ca and Sr substituted $LaCoO_3$. However, the thermodynamic stability of a perovskite phase was observed to increase when Sr was substituted for La at A-site in the lanthanum cobaltite. In the $La_{0.5}Sr_{0.5}CoO_3$ / $CaSiO_3$ sintered powder mixtures significant amounts of the perovskite like phase $Sr_{1-q}La_qCoO_{3-\delta}$ were observed to be coexistent with orthosilicates and CoO. Thus, in $La_{0.5}Sr_{0.5}CoO_3$/$CaSiO_3$ sintered powder mixtures the $LaCoO_3$-component reacts, while $SrCoO_{3-\delta}$ has a higher thermodynamic stability. Conclusively, a potential membrane material is a compromise between the kinetically stable $LaCoO_3$ and the thermodynamically more stable $SrCoO_{3-\delta}$, e.g. $La_{1-x}Sr_xCoO_{3-\delta}$. BaO is a stronger base than SrO. $BaCoO_{3-\delta}$, therefore, is thermodynamically even more stable than $SrCoO_{3-\delta}$. However, barium produces a lower oxygen ionic conductivity as a perovskite A-site dopant than strontium [31].

For industrial membrane applications it is also interesting to discuss the effect of substitution of the B-site element of the perovskite phase. A sub-

stitution of Co by Fe would presumably cause formation of a perovskite-like phase both with Ca and Sr, $(Ca, Sr)FeO_{3-\delta}$ in air, indicating an increased thermodynamic stability of a perovskite phase. However, due to the higher average oxidation number of Fe than Co [105], the pO_2-stability range is different. Taking both A- and B-site substitution of lanthanum cobaltite into consideration, a perovskite phase is expected to be stable when using $La_{1-x}Sr_xCo_{1-y}Fe_yO_{3-\delta}$ as membrane material and calcium silicate as sealing material. Thus, $La_{1-x}Sr_xCo_{1-y}Fe_yO_{3-\delta}$, which is considered as a potential membrane material due to high oxygen ionic conductivity [106], is also recommended based on the present discussion of the thermodynamic stability of the perovskite / sealant interface.

Equally important as the chemical stability of the perovskite / sealant interface is the mechanical stability of the interface. In paper VI we have studied the mechanical aspects of sealing dense oxygen permeable membranes. We conclude that the most important parameter for establishing a residual stress state in an oxygen permeable membrane system, is the difference in thermal expansion coefficient, α, (TEC) between the different components. The ideal situation is $\alpha_{\text{membrane}} \approx \alpha_{\text{sealant}} \lesssim \alpha_{\text{support}}$. Thus, the choice of support material is important even if the stress in this material is reduced to zero under the assumption that the membrane and sealant layers are much thinner than the support material. The theoretical calculations predict that *in situ* sealing of the dense ceramic membrane is necessary due to long relaxation times of the residual stress in the membrane. Sealants with suitable properties, e.g. T_g, may be designed such that the build-up of residual stress in the membrane is reduced, eventually to zero.

References

[1] U. G. Bossel, *J. Power Sources*, **57** [1-2] 141 (1995).

[2] U. Balachandran, J. T. Dusek, R. L. Mieville, R. B. Poeppel, M. S. Kleefisch, S. Pei, T. P. Kobylinski, C. A. Udovich and A. C. Bose, *Appl. Catalysis A: General*, **133** 19 (1995).

[3] A. J. Appleby and F. R. Foulkes, *Fuel Cell Handbook*, Van Nostrand Reinhold, New York, p. 579 (1989).

[4] S. C. Singhal, *Mrs. Bull.*, [March] 16 (2000).

[5] R. Stevens, *An introduction to Zirconia*, Magnesium Elektron, London, U.K., (1986).

[6] T. H. Etsell and S. N. Flengas, *Chem. Rev.*, **70** 339 (1970).

[7] E. C. Subarrarao and H. S. Maiti, *Solid State Ionics*, **11** 317 (1984).

[8] T. Takahashi, H. Iwahara and Y. Suzuki, *Proceedings of the Third Int. Symp. on Fuel Cells*, Brussels, Belgium, p. 113, (1969).

[9] C. S. Tedmon, H. S. Spacil and S. P. Mitoff, *J. Elechtrochem. Soc.*, **116** 1170 (1969).

[10] R. F. Service, *Science*, **288** 1955 (2000).

[11] S.C. Singhal and M. Dokiya, eds., *Proceedings of The Sixth Int. Symp. on Solid Oxide Fuel Cells*, The Electrochemical Society, Pennington, NJ, (1999).

[12] J. A. Kilner and B. C. H. Steele, *Nonstoichiometric Oxides*, Academic Press, New York, p. 233 (1981).

[13] R. M. Dell and A. Hooper, *Solid Electrolytes*, Academic Press, New York, p. 291 (1978).

[14] B. C. H. Steele, *J. Power Sources*, **49** 1 (1994).

[15] C. Milliken, S. Guruswamy and A. Khandkar, *J. Elecrochem. Soc.*, **146** 872 (1999).

[16] T. Hibino, A. Hashimoto, T. Inoue, J. Tokuno, S. Yoshida and M. Sano, *Science*, **288** 2031 (2000).

[17] H. J. M. Bouwmeester and A. J. Burgraaf, *Fundamentals of Inorganic Membrane Science and Technology*, Elsevier, Amsterdam, p. 435-528 (1996).

[18] T. J. Mazanec, *Solid State Ionics*, **70/71** 11 (1994).

[19] S. Carter, A. Selcuk, R. J. Chater, J. Kajda, J. A. Kilner and B. C. H. Steele, *Solid State Ionics*, **53-56** 597 (1992).

[20] V. V. Kharton, E. N. Naumovich and A. V. Nikolaev, *J. Membr. Sci.*, **111** 149 (1996).

[21] L. Qiu, T. H. Lee, L. Y. L. Yang, A. J. Jacobson and L.-M. Liu, *Solid State Ionics*, **76** 321 (1995).

[22] R. M. Thorogood, R. Srinivasan, T. F. Yu, M. P. Drake, US Patent 5,240,480 (1993).

[23] V. V. Kharton, A. V. Nikolaev, E. N. Naumovich and V. V. Samokhval, *Inorg. Mater.*, **30** 492 (1994).

[24] V. V. Kharton, V. N. Tikhonovich, E. A. V. Kovalevsky, A. P. Viskup, I. A. Bashmakov and A. A. Yaremchenko, *J. Electrochem. Soc.*, **145** 1363 (1998).

[25] A. V. Kovalevsky, V. V. Kharton, V. N. Tikhonovich, E. N. Naumovich, A. A. Tonoyan, O. P. Reut and L. S. Boginsky, *Mater. Sci. Eng.*, **B 52** 105 (1998).

[26] V. V. Kharton, A. A. P. Viskup, E. N. Naumovich and A. A. Tonoyan, *Mater. Chem. Phys.*, **53** 6 (1998).

[27] Y. Teraoka, T. Nobunaga, K. Okamoto, N. Miura and N. Yamazoe, *Solid State Ionics*, **48** [3-4] 207 (1991).

[28] Y. Teraoka, H. M. Zhang, K. Okamoto and N. Yamazoe, *Mat. Res. Bull.*, **23** [1] 51 (1988).

[29] Y. Teraoka, H. M. Zhang, S. Furukawa and N. Yamazoe, *Chem. Lett.*, 1743 (1985).

[30] C. Tsai, A. G. Dixon, Y. H. Ma, W. R. Moser and M. Pascucci, *J. Am. Ceram. Soc.*, **81** 1437 (1998).

[31] J. W. Stevenson, T. R. Armstrong, L. R. Pederson and W. J. Weber, *The First Int. Symp. on Ceramic Membranes*, Edited by H. U. Anderson, A. C. Khandkar and M. Liu, p. 94, (1995).

[32] J. Mizusaki, H. Tagawa, K. Tsuneyoshi and A. Sawara, *J. Electrochem. Soc.*, **138** [7] 1867 (1991).

[33] J. Mizusaki, H. Tagawa, K. Tsuneyoshi, A. Sawara, M. Katou and K. Hirano, *Denki Kagaku*, **58** [6] 520 (1990).

[34] Y. Takeda, Y. Sakai, T. Ichikawa, N. Imanishi and O. Yamamoto, *Solid State Ionics*, **72** 257 (1994).

[35] H. Taimatsu, K. Wada, H. Kaneko and H. Yamamura, *J. Am. Ceram. Soc.*, **75** 401 (1992).

[36] J. A. M. van Roosmalen and E. H. P. Cordfunke, *Solid State Ionics*, **52** 303 (1992).

[37] G. Stochniol, E. Syskakis and A. Noumidis, *J. Am. Ceram. Soc.*, **78** 929 (1995).

[38] K. Wiik, C. R. Schmidt, S. Faaland, S. Shamsili, M.-A. Einarsrud and T. Grande, *J. Am. Ceram. Soc.*, **82** [3] 721 (1999).

[39] K. Kleveland, M.-A. Einarsrud, C. R. Schmidt, S. Shamsili, S. Faaland, K. Wiik and T. Grande, *J. Am. Ceram. Soc.*, **82** [3] 729 (1999).

[40] P. S. Maiya, U. Balachandran, J. T. Dusek, R. L. Mieville, M. S. Kleefisch and C. A. Udovich, *Solid State Ionics*, **99** 1 (1997).

[41] A. M. Glazer, *Acta Cryst.*, **A 31** 756 (1975).

[42] V. M. Goldschmidt, Skr. Nor. Vidensk.-Akad. [K1] 1: Mat.-Naturvidensk. K1 No. 2 (1926).

[43] B. C. Tofield and W. R. Scott, *J. Solid State Chem.*, **14** 395 (1974).

[44] J. A. M. van Roosmalen, E. H. P. Cordfunke, R. B. Helmholdt and H. W. Zandbergen, *J. Solid State Chem.*, **110** 100 (1994).

[45] P. D. Battle, T. C. Gibb and C. W. Jones, *J. of Solid State Chem.*, **74** 60 (1988).

[46] T. Negas and R. S. Roth, *J. of Solid State Chem.*, **1** 409 (1970).

[47] K. R. Poeppelmeier, M. E. Leonowicz, J. C. Scanlon, J. M. Longo and W. B. Yelon, *J. Solid State Chem.*, **45** 71 (1982).

[48] A. K. Bogush, V. I. Pavlov and L. V. Balyko, *Crystal Res. and Technol.*, **18** [5] 589 (1983).

[49] P. G. Radaelli, D. E. Cox, M. Marezio, S.-W. Cheong, P. E. Schiffer and A. P. Ramirez, *Phys. Rev. Lett.*, **75** [24] 4488 (1995).

[50] G. Thornton, B. C. Tofield and A. W. Hewat, *J. Solid State Chem.*, **61** 301 (1986).

[51] A. Mineshige, M. Inaba, T. Yao, Z. Ogumi, K. Kikuchi and M. Kawase, *J. Solid State Chem.*, **121** 423 (1996).

[52] E. Woermann and A. Muan, *J. Inorg. Nucl. Chem.*, **32** [5] 1457 (1970).

[53] J. H. Kuo, H. U. Anderson and D. M. Sparlin, *J. Solid State Chem.*, **83** 52 (1989).

[54] J. H. Kuo, H. U. Anderson and D. M. Sparlin, *J. Solid State Chem.*, **78** 55 (1990).

[55] J. Mizusaki, Y. Mima, S. Yamauchi, K. Fueki and H. Tagawa, *J. Solid State Chem.*, **80** 102 (1989).

[56] A. N. Petrov, V. A. Cherepanov, O. F. Konochuk and L. Y. Gavrilova, *J. Solid State Chem.*, **87** 69 (1990).

[57] H. Kruidhof, H. J. M. Bouwmeester, R. H. E. VonDoorn and A. J. Burggraaf, *Solid State Ionics*, **63-65** 816 (1993).

[58] O. Yamamoto, Y. Tekeda, R. Kanno and M. Noda, *Solid State Ionics*, **22** 241 (1987).

[59] Y. Ohno, S. Nagata and H. Sato, *Solid State Ionics*, **3/4** 439 (1981).

[60] H. Lauret, E. Caignol and A. Hammou, *Proceedings of the Second International Symposium on Solid Oxide Fuel Cells*, Luxembourg, Edited by F. Gross, P. Zegers, S. C. Singhal and O. Yamamoto, p. 479, (1991).

[61] H. Schmalzried, *Chemical Kinetics of Solids*, VCH, Weinheim, p. 153 (1995).

[62] C. Wagner, *Z. Phys. Chem. B*, **21** 25 (1933).

[63] C. Wagner, *Z. Phys. Chem. B*, **32** 447 (1936).

[64] N. Q. Minh, *J. Am. Ceram. Soc.*, **76** [3] 563 (1993).

[65] H. Yokokawa, N. Sakai, T. Kawada and M. Dokiya, *Denki Kagaku*, **57** 821 (1989).

[66] H. Yokokawa, N. Sakai, T. Kawada and M. Dokiya, *Denki Kagaku*, **57** 829 (1989).

[67] H. Yokokawa, N. Sakai, T. Kawada and M. Dokiya, *Denki Kagaku*, **58** 161 (1990).

[68] H. Yokokawa, N. Sakai, T. Kawada and M. Dokiya, *Denki Kagaku*, **58** 489 (1990).

[69] H. Yokokawa, N. Sakai, T. Kawada and M. Dokiya, *Solid State Ionics*, **40/41** 398 (1990).

[70] H. Yokokawa, N. Sakai, T. Kawada and M. Dokiya, *J. Electrochem. Soc.*, **138** 1018 (1991).

[71] H. Yokokawa, N. Sakai, T. Kawada and M. Dokiya, *J. Electrochem. Soc.*, **138** 2719 (1991).

[72] H. Yokokawa, N. Sakai, T. Kawada and M. Dokiya, *J. Electrochem. Soc.*, **138** [9] 2719 (1991).

[73] H. Yokokawa, N. Sakai, T. Kawada and M. Dokiya, *Solid State Ionics*, **52** 43 (1992).

[74] H. Yokokawa, N. Sakai, T. Kawada and M. Dokiya, *Sci. Tech. Zirconia*, **5** 752 (1993).

[75] J. A. M. van Roosmalen and E. H. P. Cordfunke, *J. Solid State Chem.*, **110** 109 (1994).

[76] J. A. M. van Roosmalen and E. H. P. Cordfunke, *J. Solid State Chem.*, **93** 212 (1991).

[77] J. A. M. van Roosmalen, E. H. P. Cordfunke and J. P. P. Huijsmans, *Solid State Ionics*, **66** 285 (1993).

[78] J. A. M. van Roosmalen and E. H. P. Cordfunke, *J. Solid State Chem.*, **110** 106 (1994).

[79] J. A. M. van Roosmalen and E. H. P. Cordfunke, *J. Solid State Chem.*, **110** 117 (1994).

[80] C. Evju, 'Sintring av kalsium og strontium dopet lantanmanganitt', Diploma thesis, Department of Inorganic Chemistry, NTNU (1996).

[81] G. Watterud, 'Sintring av keramiske materialer aktuelle som oksygen permeable membraner', Diploma thesis, Department of Inorganic Chemistry, NTNU (1997).

[82] J. A. M. van Roosmalen, J. P. P. Huijsmans and L. Plomp, *Solid State Ionics*, **66** 279 (1994).

[83] J. C. C. Abrantes, C. M. S. Rodrigues, J. A. Labrincha, J. R. Frade and J. M. B. Marques, *Ceramic oxygen ion conductors and their technological applications, British Ceramic Proceedings*, Edited by B. C. H. Steele, p. 125, (1992).

[84] D. W. Richerson, *Modern Ceramic Engineering*, Marcel Dekker, Inc., New York, (1992).

[85] J. A. Pask, *Ceramic Bulletin*, **66** [11] 1587 (1987).

[86] D. W. J. Schmidt, *J. Chem. Educ.*, **64** 480 (1987).

[87] Y.-K. Lee and J.-W. Park, *Materials Chemistry and Physics*, **45** 97 (1996).

[88] T. Horita, N. Sakai, T. Kawada, H. Yokokawa and M. Dokiya, *Denki Kagaku*, **61** [7] 760 (1993).

[89] P. H. Larsen and P. F. James, *J. Mat. Sci.*, **33** 2499 (1998).

[90] P. H. Larsen, S. Primdahl and M. Mogensen, *Proceedings of the 17th Risø Int. Symp. on Materials Science*, Risø national Laboratory, Roskilde, Denmark, Edited by F. W. Poulsen, N. Bonanos, S. Linderoth, M. Mogensen and B. Zachau-Christiansen, p. 331, (1996).

[91] T. Horita, J.-S. Sam, Y.-K. Lee, N. Sakai, T. Kawada, H. Yokokawa and M. Dokiya, *J. Am. Ceram. Soc.*, **78** [7] 1729 (1995).

[92] T. Yamamoto, H. Itoh, M. Mori, N. Mori and T. Watanabe, *Denki Kagaku*, **64** [6] 575 (1996).

[93] V. V. Kharton, A. A. Yaremchenko, A. V. Kovalevsky, A. P. Viskup, E. N. Naumovich and P. F. Kerko, *J. Membrane Sci.*, **163** 307 (1999).

[94] I. W. Donald, *J. Mat. Sci.*, **28** 2841 (1993).

[95] H. U. Anderson, *Solid State Ionics*, **52** 33 (1992).

[96] P. V. Hendriksen, P. H. Larsen, M. Mogensen, F. W. Poulsen and K. Wiik, *Catalysis Today*, **56** 283 (2000).

[97] U. Balachandran, J. T. Dusek, S. M. Sweeney, R. B. Poebbel, R. L. Mieville, P. S. Mayia, M. S. Kleefisch, S. Pei, T. P. Kobylinski, C. A. Udovich and A. Bose, *Am. Ceram. Soc. Bull.*, **74** 71 (1995).

[98] S. Pei, M. S. Kleefisch, T. P. Kobylinski, J. Faber, C. A. Udovich, V. Zhang-McCoy, B. Dabrowski, U. Balachandran, R. L. Mieville and R. B. Poeppel, *Catalysis Lett.*, **30** 201 (1995).

[99] W. Laqua and H. Schmalzried, *Chemical Metallurgy - A Tribute to Carl Wagner*, Metallurgical Society of AIME, Warrendale, PA, Edited by N. A. Gokcen, p. 29, (1981).

[100] H. Schmalzried, W. Laqua and P. L. Lin, *Z. Naturforsch., A*, **34** [2] 192 (1979).

[101] R. L. Shultz and A. Muan, *J. Am. Ceram. Soc.*, **54** 504 (1971).

[102] D. W. Smith, *J. Chem. Educ.*, **64** 480 (1987).

[103] S. Mukhopadhyay and K. Jacob, *American Mineralogist*, **81** 963 (1996).

[104] R. A. Robie, B. S. Hemingway and J. R. Fisher, *Thermodynamic Properties of Minerals and Related Substances at 298.15 K and 1 Bar (*10^5 *Pascals) Pressure and at Higher Temperatures*, United States Government Printing Office, Washington, (1978).

[105] D. P. Masse and A. Muan, *J. Am. Ceram. Soc.*, **48** [9] 467 (1965).

[106] Y. Teraoka, H. M. Zhang, K. Okamoto and N. Yamazoe, *Mater. Res. Bull.*, **23** 51 (1988).

The following papers are not included in the pdf-file due to copyright restrictions:

Paper I S. Faaland, K.D. Knudsen, M.-A. Einarsrud, L. Rørmark, R. Høier, T. Grande: Structure, Stoichiometry, and Phase Purity of Calcium Substituted Lanthanum Manganite Powders, *J. Solid State Chem.*, **140**, 320 (1998).
doi:10.1006/jssc.1998.7894

Paper II S. Faaland, M.-A. Einarsrud, K. Wiik, R. Høier, T. Grande: Reaction between $La_{1-x}Ca_xMnO_3$ and CaO-stabilized ZeO_2, Part I: powder mixtures, *J. Mat. Sci.*, **34**, 957 (1999).
doi: 10.1023/A:1004527508004

Paper III S. Faaland, M.-A. Einarsrud, K. Wiik, R. Høier, T. Grande: Reaction between $La_{1-x}Ca_xMnO_3$ and CaO-stabilized ZeO_2, Part II: Diffusion Couples, *J. Mat. Sci.*, **34**, 5811 (1999).
doi: 10.1023/A:1004766419921

Paper IV S. Faaland, M.-A. Einarsrud, R. Høier: Reaction between $La_{1-x}Ca_xMnO_3$ (x=0.3 and 0.6) and CaO-stabilized ZRO_2 powder mixtures studied on a nano-meter scale, *J. Mat. Sci. Lett.*, **19** [15], 1379 (2000).
doi: 10.1023/A:1006765502504

Paper V S. Faaland, M.-A. Einarsrud, T.Grande: Reactions between calcium and strontium substituted cobaltite ceramic membranes and calcium silicate sealing materials, *Chem. of Mat.*, **13** [3], 723 (2001).
doi: 10.1021/cm991184n

Appendices A and B:

Paper VII K. Wiik, C.R. Schmidt, S. Faaland, S. Shamsili, M.-A. Einarsrud, T. Grande: Reactions between Strontium-Substituted Lanthanum Manganite and Yttria-Stabilized Zirconia: I, Powder Samples, *J. Am. Ceram. Soc.*, **82** [3], 721 (1999).
doi:10.1111/j.1151-2916.1999.tb01823.x

Paper VIII K. Kleveland, M.-A. Einarsrud, C.R. Schmidt, S. Shamsili, S. Faaland, K. Wiik, T. Grande: Reactions between Strontium-Substituted Lanthanum Manganite and Yttria-Stabilized Zirconia: II, Diffusion Couples, *J. Am. Ceram. Soc.* **82** [3], 729 (1999).
doi:10.1111/j.1151-2916.1999.tb01824.x

Paper VI

Mechanical Aspects of Sealing Dense Oxygen Permeable Membranes

Sonia Faaland
Department of Chemistry,
Norwegian University of Science and Technology
7491 Trondheim, Norway

November 6, 2000

1 Introduction

Dense, oxygen permeable, ceramic membranes can be used for direct conversion of methane to syngas and for separation of oxygen from air. Mixed conducting perovskite oxides are potential membrane materials. Ceramic membranes can be shaped into a hollow-tube reactor, over which air flows on the outside of the membrane and methane flows through the inside (Fig. 1). Honeycomb or corrugated reactors are also possible. However, regardless of the membrane design, a gas-tight seal between membrane and support is essential.

In dense oxygen permeable membrane systems residual stresses are developed in membrane, sealant and support due to the temperature change during the sealing process and operation of the membrane. Residual stresses might arise due to a mismatch in thermal expansion coefficients (TEC) because the materials are bonded together and each one restricts the ability of the other to reach its equilibrium (zero stress) size. In addition, chemical lattice expansion / contraction due to interdiffusion of cations or changes of oxygen partial pressure can result in significant residual stresses. For the acceptor doped perovskite materials it is known that the unit cell volume changes with changes of oxygen stoichiometry [1, 2] and thereby with changes in pO_2. In general, the membrane is not free to deform according to any pO_2-profile, and therefore the volume expansion / contraction will lead to a build-up of mechanical stresses. Evidently, one must know the

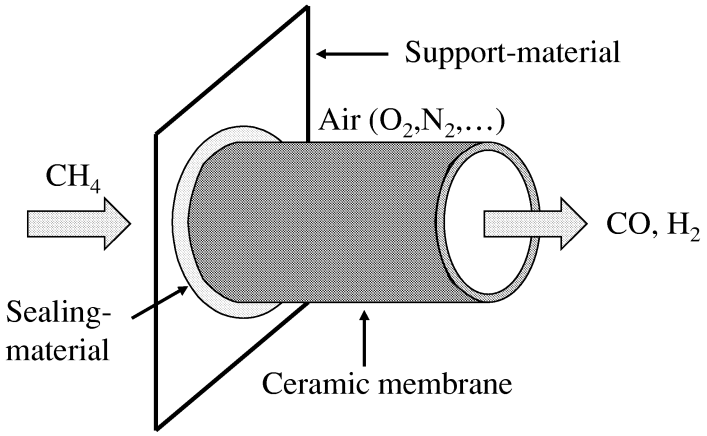

Figure 1: Schematic drawing of an oxygen permeable membrane system.

lattice expansion induced strain profile in the membrane material. In addition to residual stress due to thermal and chemical expansion, formation of undesirable reaction products at the membrane / sealant interface may alter the mechanical properties of the interface. This last mentioned effect will not be discussed any further here.

Residual stresses can be relaxed due to creep; the mechanism of creep being dependent on the type of material. The mechanism of creep in ceramic materials is the movement of dislocations through the crystal structure (single crystal) and diffusion or grain boundary sliding (polycrystalline ceramics). Creep in glasses is controlled by viscous flow and is a function of the viscosity of the glass at the temperature of interest. Under the action of applied stress, a viscous material will flow. Of importance to relaxation of residual stress in glasses are the softening and glass transition temperatures, T_s and T_g. The viscosities associated with these temperatures for all glasses are, respectively, $10^{7.6}$ P and 10^{13} P [3]. Above T_s the material deforms in a short time to relieve any stresses which are imposed. As the temperature is lowered, a point will be reached (T_g) where stress relaxation of the glass becomes so slow that any differences in thermal contraction between the two materials can no longer be accommodated. A further decrease in temperature will then result in the creation, within the time-scales involved, of residual stress.

A desired property of a sealing material is the ability to seal by viscous flow. Silicate glasses are potential sealing materials. For example, the viscosity of

$CaSiO_3$ at 1000°C is $\sim 10^5$ P [4] (above softening temperature), enabling viscous flow at 1000°C. Thus, 1000°C is a suitable sealing temperature. The glass transition temperature, T_g, of $CaSiO_3$ is 770°C [5]. Hence, stress relaxation of the glass will occur at the operating temperature of the membrane (800-900°C [6, 7]), and $CaSiO_3$ is a promising sealant. For silicate glasses the viscosity decreases with increasing concentration of modifying cations [3]. Thus, Ca_2SiO_4 has a lower viscosity than $CaSiO_3$. In contrast to alkali and alkali earth oxides, additions of Al_2O_3 increase the viscosity.

The build-up of residual stresses might cause delamination and/or tunnel cracking of the membrane system. Tunnel cracking has been observed in $La_{1-x}(Ca/Sr)_xCoO_3$(LMC) / $CaSiO_3$ diffusion couples [8]. Both delamination and cracking may result in gas-leakage, which must be prohibited.

The aim of the present investigation is to perform a calculation of the permanent stresses at interfaces in dense oxygen permeable membrane systems and to identify important parameters determining possibility for failure. Different membrane, sealing and support materials will be considered. The effect on the residual stress of lattice expansion / contraction of the membrane due to variation in oxygen stoichiometry with changes in pO_2 is discussed. Relaxation times of the residual stresses due to the cooling process from the sealing temperature are calculated.

2 Derivation of Equations for Residual Stresses in Multilayer Systems

To be able to calculate the magnitude of the residual stresses in oxygen permeable membrane systems, a simplified model can be assumed (Fig. 2). Several authors have presented calculations for laminated composites using the simple beam bending theory (bimaterial strip problem) [9–13] or by using the force balance approach [14–17]. The last mentioned method is mostly used for symmetric composites (uneven number of layers of two different materials, 121 etc.). However, the force balance approach can be generalized to an asymmetric composite (random number of layers of different materials, 123 etc.) as shown below. In oxygen permeable membrane systems, where the layer of support material is thick, bending is not possible, i.e. the strain is constant in the whole composite. Since the layers are considered as isotropic and linearly elastic [1], Hooke's law for an in-plane

[1] Several possible membrane materials are ferroelastic, giving a non-elastic behaviour.

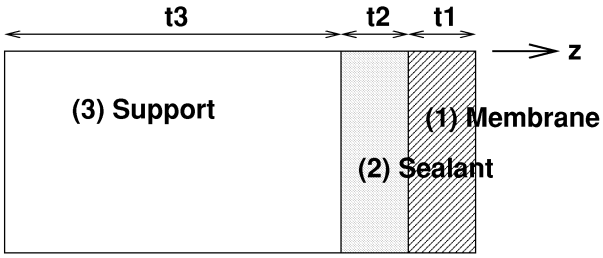

Figure 2: Schematic drawing of the interfaces in oxygen permeable membrane systems.

stress state can be applied to this system. The stress normal to the membrane surface is equal to zero, i.e. $\sigma_z = 0$. The x- and y-directions are equivalent, i.e. $\sigma_x = \sigma_y$. This means that the elastic stresses in the layers can be expressed as:

$$\sigma_i = \frac{E_i}{1-\nu_i}(\epsilon_i - \alpha_i \Delta T) \tag{1}$$

where i is a layer index, E is Young's modulus, ν is Poisson's ratio, α is thermal expansion coefficient (TEC) and T is absolute temperature. ϵ is the overall biaxial strain, i.e. the actual expansion of a volume-element, when it is not allowed to expand freely, but is constrained as part of an elastic body. $\alpha\Delta T$ is the thermal strain. Thus, the strains in each layer are given as:

$$\epsilon_i = \frac{1-\nu_i}{E_i}\sigma_i + \alpha_i \Delta T \tag{2}$$

In an asymmetric three layer composite, where all layers have the same strain:

$$\epsilon_1 = \epsilon_2 = \epsilon_3 \tag{3}$$

Thus, we get two independent equations:

$$\frac{1-\nu_1}{E_1}\sigma_1 + \alpha_1 \Delta T = \frac{1-\nu_2}{E_2}\sigma_2 + \alpha_2 \Delta T \tag{4}$$

$$\frac{1-\nu_2}{E_2}\sigma_2 + \alpha_2 \Delta T = \frac{1-\nu_3}{E_3}\sigma_3 + \alpha_3 \Delta T \tag{5}$$

Since no deformation occurs, i.e. the stress does not vary as a function of

z in a given material, the force balance requires that:

$$\sum_{i=1}^{3} \sigma_i t_i = 0 \tag{6}$$

where σ_i is the stress and t_i the thickness of material i (i=1 membrane, i=2 sealant, i=3 support). Solving the three equations 4, 5 and 6 for the three unknowns σ_1, σ_2 and σ_3, we get:

$$\sigma_1 = -\frac{\Delta T\left((\alpha_1-\alpha_2)\frac{E_2 t_2}{(1-\nu_2)} + (\alpha_1-\alpha_3)\frac{E_3 t_3}{(1-\nu_3)}\right)}{t_1 + \frac{(1-\nu_1)}{(1-\nu_2)}\frac{E_2 t_2}{E_1} + \frac{(1-\nu_1)}{(1-\nu_3)}\frac{E_3 t_3}{E_1}} \tag{7}$$

$$\sigma_2 = -\frac{\Delta T\left((\alpha_2-\alpha_1)\frac{E_1 t_1}{(1-\nu_1)} + (\alpha_2-\alpha_3)\frac{E_3 t_3}{(1-\nu_3)}\right)}{t_2 + \frac{(1-\nu_2)}{(1-\nu_1)}\frac{E_1 t_1}{E_2} + \frac{(1-\nu_2)}{(1-\nu_3)}\frac{E_3 t_3}{E_2}} \tag{8}$$

$$\sigma_3 = -\frac{\Delta T\left((\alpha_3-\alpha_2)\frac{E_2 t_2}{(1-\nu_2)} + (\alpha_3-\alpha_1)\frac{E_1 t_1}{(1-\nu_1)}\right)}{t_3 + \frac{(1-\nu_3)}{(1-\nu_1)}\frac{E_1 t_1}{E_3} + \frac{(1-\nu_3)}{(1-\nu_2)}\frac{E_2 t_2}{E_3}} \tag{9}$$

Assuming the membrane and the sealant layers are much thinner than the support material, $t_1 << t_3$ and $t_2 << t_3$, these equations simplify to:

$$\sigma_1 = -\frac{\Delta T(\alpha_1-\alpha_3)}{\frac{1-\nu_1}{E_1}} \tag{10}$$

$$\sigma_2 = -\frac{\Delta T(\alpha_2-\alpha_3)}{\frac{1-\nu_2}{E_2}} \tag{11}$$

$$\sigma_3 = 0 \tag{12}$$

Residual stress can be induced not only due to thermal expansion mismatch but also due to lattice expansion / contraction due to variation in oxygen stoichiometry with changes in pO_2. In the following, this lattice expansion is called chemical expansion. The biaxial stress field developing in a membrane due to the chemical expansion induced strain, $\epsilon_{i,ch}$, is given by Eq. 1 by substituting $\epsilon_{i,ch}$ for the thermal expansion, $\alpha_i \Delta T_i$:

$$\sigma_i = \frac{E_i}{1-\nu_i}(\epsilon - \epsilon_{i,ch}) \tag{13}$$

A similar derivation as made for thermal expansion is made for the chemical expansion to reach the residual stress:

$$\sigma_{1,ch} = -\frac{\frac{E_2 t_2}{(1-\nu_2)}\epsilon_{1,ch} + \frac{E_3 t_3}{(1-\nu_3)}\epsilon_{1,ch}}{t_1 + \frac{E_2 t_2}{E_1}\frac{(1-\nu_1)}{(1-\nu_2)} + \frac{E_3 t_3}{E_1}\frac{(1-\nu_1)}{(1-\nu_3)}} \tag{14}$$

It is assumed that there is no lattice expansion in the sealant. Assuming the membrane and the sealant layers are much thinner than the support material, $t_1 << t_3$ and $t_2 << t_3$, the equation simplifies to

$$\sigma_{1,ch} = -\frac{\epsilon_{1,ch} E_1}{(1-\nu_1)} \tag{15}$$

3 Case-study: Sealing Dense Oxygen Permeable Membranes

The preparation of dense oxygen permeable membrane systems includes heating the membrane, followed by a sealing process at a suitable sealing temperature. The system is subsequently cooled to room temperature (Fig. 3a). With sealing process is meant sealing the membrane to the support. A suitable sealing temperature is a temperature close to the softening point of the sealant. For example, 1000°C is a suitable sealing temperature for $CaSiO_3$ glass. Thus, in the following 1000°C is taken as the sealing temperature. The operation of dense oxygen permeable membrane systems includes a heating followed by residence at the operating temperature of the membrane (Fig. 3b). Teraoka et al. [6,7] have shown that perovskites in the La-Sr-Fe-Co-O system exhibit oxygen ionic and electronic conductivity and appreciable oxygen permeability at ∼800°C. Thus, in the following the operating temperature is set equal to 800°C. There will be a stress build-up in the components of the membrane system due to both preparation and operation (Fig. 3a,b). To reduce the temperature interval for stress build-up, the sealing process could be done *in situ*. With *in situ* sealing is meant cooling the sealed system directly from the sealing temperature to the operating temperature (Fig. 3c).

Thermal expansion coefficients (TEC) of selected membrane materials, sealants and support materials are shown in Table 1, and mechanical properties of selected perovskite materials are given in Table 2. $La_{0.8}Ca_{0.2}CoO_3$, $La_{0.8}Sr_{0.2}Co_{0.2}Fe_{0.8}O_3$ and $La_{0.6}Sr_{0.4}Co_{0.2}Fe_{0.8}O_3$ are mixed conducting oxides. Thus, a typical membrane material has a bend strength of approximately 160 MPa at room temperature. A rule of thumb says that a material can withstand a compressive stress in the order of 10 times a tensile stress [18]. Bend strength of different experimental test geometries (three-point, four-point, biaxial etc.) lies between compressive- and tensile strength, closer to the latter.

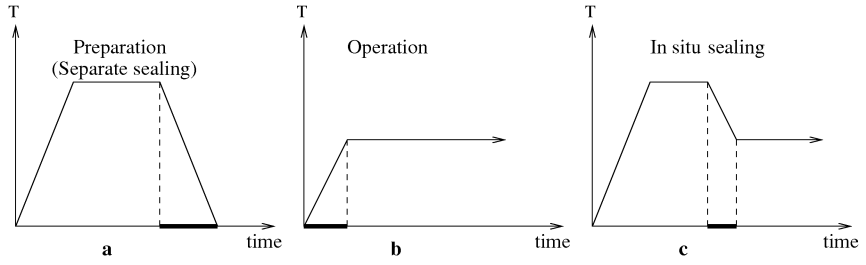

Figure 3: Schematic drawing of the temperature program for preparation, operation and *in situ* sealing of dense oxygen permeable membranes. The bold lines at the abscissa indicate periods for possible build-up of residual stresses.

Residual membrane stresses due to preparation (separate sealing, Fig. 3a) were calculated from Eq. 10 and are given in Table 3, using $LaCrO_3$ as support material and assuming no relaxation of stress. Hence, the stress values in Table 3 are upper limits. Maximum residual stresses from *in situ* sealing (Fig. 3c) are also included in Table 3. The build-up of residual stress due to the heating process to the operating temperature (Fig. 3b) has not been calculated because of the unknown stress-state at room temperature. Poisson's ratio and Young's modulus for all membrane materials were set equal to, respectively, 0.3 and 100 GPa, which are typical values for ceramic materials [3]. The magnitude of the residual stress is significantly larger for separate sealing than for *in situ* sealing. Due to a decreasing temperature and a smaller TEC of the support material ($LaCrO_3$), all membranes, except $LaFe_{0.8}Ni_{0.2}O_{3-\delta}$, are in tension. Among the other membranes, $Sr_{1.05}FeO_{3-\delta}$ causes the lowest tensile stress. Hence, only the ferrites are supposed to resist cracking due to preparation, assuming a bend strength of 160 MPa. However, by performing the sealing process *in situ*, even $SrCoO_{3-\delta}$ is likely to resist cracking.

The build-up of residual stress in the sealant is more complex than the build-up of stress in the ceramic membrane, because the assumption of no relaxation of stress is poor above T_g. However, residual sealant stresses due to preparation (separate sealing) and *in situ* sealing are given in Table 3, using $LaCrO_3$ as support material and assuming no relaxation of stress. Stress-relief is discussed in a following section.

Table 1: Thermal expansion coefficient (TEC) for selected membrane-, sealing- and support materials.

	TEC $\alpha \cdot 10^6$ [K^{-1}]	Temperature interval	Reference
(1) Membrane			
$LaCoO_{3-\delta}$	22.9	27-827°C	[19]
$SrCoO_{3-\delta}$	13	27-827°C	[20]
$Sr_{1.05}FeO_{3-\delta}$	∼10	25-600°C	[21]
$SrFe_{0.5}Co_{0.5}O_{3-\delta}$	18	27-477°C	[22]
$LaFe_{0.8}Ni_{0.2}O_{3-\delta}$	8.9	27-827°C	[23]
$LaMnO_{3\pm\delta}$ †	11.2	25-1100°C	[24]
(2) Sealant (glass)			
Ca_2SiO_4	13.8	300-400°C	[5]
$CaSiO_3$	10.5	300-400°C	[5]
$SrSiO_3$	∼12	300-400°C	[5]
$BaSiO_3$	∼12	300-400°C	[5]
$NaAlSiO_4$	8	20-100°C	[25, 26]
$CaAl_2Si_2O_8$	6.8	20-300°C	[27, 28]
$K_4Al_2Si_{14}O_{33}$	6.5	0-300°C	[29]
Pyrex	3.3	0-300°C	[30]
(3) Support			
Al_2O_3	8.1	average TEC	[31]
MgO	∼ 10	average TEC	[3]
ZrO_2	∼ 10	average TEC	[3]
YSZ	10.3	25-1100°C	[24]
$LaCrO_3$	9.5	25-1100°C	[24]
$La_{0.9}Mg_{0.1}CrO_3$ ‡	9.5	25-1100°C	[24]
$La_{0.98}Sr_{0.02}CrO_3$ ‡	10.2	25-1100°C	[24]
$LaCr_{0.9}Co_{0.1}O_3$ ‡	13.1	25-1100°C	[24]
$LaCr_{0.7}Co_{0.3}O_3$ ‡	15.9	25-1100°C	[24]
$La_{0.9}Ca_{0.1}Cr_{0.9}Co_{0.1}O_3$ ‡	12.3	25-1100°C	[24]
$La_{0.7}Ca_{0.3}Cr_{0.9}Co_{0.1}O_3$ ‡	10.4	25-1100°C	[24]

†Not a realistic membrane material due to low oxygen permeability.

‡Not a realistic support material due to mixed electronic and oxygen ionic conductivity.

Table 2: Mechanical properties of perovskite materials at room-temperature. Numbers in parentheses represent standard deviations.

Material	Bend strength [MPa]	Young's modulus [GPa]	Experimental test geometry	Reference
$LaCoO_3$	53[†]	83(3)	4-point	[32]
$La_{0.8}Ca_{0.2}CoO_3$	150[†]	112(3)	4-point	[32]
$La_{0.8}Sr_{0.2}CoO_3$	76[†]	86(13)	4-point	[32]
$La_{0.875}Sr_{0.125}MnO_3$	164	-	3-point	[33]
$La_{0.8}Sr_{0.2}Co_{0.2}Fe_{0.8}O_3$	165	161(2)	biaxial[‡]	[34]
$La_{0.6}Sr_{0.4}Co_{0.2}Fe_{0.8}O_3$	155	152(3)	biaxial[‡]	[34]
$La_{0.4}Sr_{0.6}Co_{0.2}Fe_{0.8}O_3$	50	167(9)	biaxial[‡]	[34]
$La_{0.2}Sr_{0.8}Co_{0.2}Fe_{0.8}O_3$	40	188(6)	biaxial[‡]	[34]
$BaTiO_3$	93	110 [35]	4-point	[36]
$LaCr_{0.9}Mg_{0.1}O_3$	140	-	4-point	[37]
$La_{0.9}Sr_{0.1}Ga_{0.8}Mg_{0.2}O_3$	162	-	biaxial[‡]	[38]
$La_{0.8}Sr_{0.2}Ga_{0.8}Mg_{0.2}O_3$	150	190	biaxial[‡]	[39]
$La_{0.75}Ca_{0.25}CrO_3$	120	-	4-point	[40]
$La_{0.7}Sr_{0.3}CrO_3$	234	-	3-point	[41]
$La_{0.7}Ca_{0.3}CrO_3$	256	-	3-point	[41]
$La_{0.8}Sr_{0.2}CrO_3$	75[$]	-	3-point	[42]
$La_{0.8}Ca_{0.2}CrO_3$	57[$]	-	3-point	[42]

[†] Fracture origin was large voids, giving a higher strength of a material without defects.

[‡] Ball(s)-on-ring geometry

[$] At 1000°C

For a thermal expansion of the support material larger than the thermal expansion of both membrane and sealant, both membrane and sealant will be in compression during the cooling process from the sealing temperature. For oxygen permeable membrane systems, this situation is favourable. The ideal situation is $\alpha_{\text{membrane}} \approx \alpha_{\text{sealant}} \lesssim \alpha_{\text{support}}$. Thus, sealing and support materials with thermal expansion coefficients minimizing the stress / inverting the sign of the stress could be designed. The TEC of $LaCrO_3$ can be modified by substitution of cations at A- and/or B-site in the perovskite structure (Table 1). Exclusive A-site substitution (Ca,Sr) increases the TEC, while exclusive B-site substitution (Al,Co) increases the TEC even more markedly. However, a combination of A-site and B-site substitution

Table 3: Maximum residual stresses [MPa] in membranes and sealants, using $LaCrO_3$ as support material and assuming no relaxation of stress. Poisson's ratio and Young's modulus were set equal to, respectively, 0.3 and 100 GPa for all membrane materials. For the sealants, typical glass parameters, ν=0.2 and E=69 GPa [3] were used. 'Total' residual stresses for *in situ* sealing include stress from chemical expansion during operation, assuming no cracking before the membrane is in operation.

	Maximum residual stress [MPa] from		
Membrane	preparation (separate sealing) ΔT=-980K	*in situ* sealing ΔT=-200K	*in situ* sealing 'total' stress ΔT=-200K
$LaCoO_{3-\delta}$	1876	383	-117
$SrCoO_{3-\delta}$	490	100	-400
$Sr_{1.05}FeO_{3-\delta}$	70	14	-486
$SrFe_{0.5}Co_{0.5}O_{3-\delta}$	1190	243	-257
$LaFe_{0.8}Ni_{0.2}O_{3-\delta}$	-84	-17	-517
$LaMnO_{3\pm\delta}$	238	49	-451
Sealant			
Ca_2SiO_4	363	74	
$CaSiO_3$	85	17	
$SrSiO_3$	211	43	
$BaSiO_3$	211	43	
$NaAlSiO_4$	-127	-26	
$CaAl_2Si_2O_8$	-228	-46	
$K_4Al_2Si_{14}O_{33}$	-254	-52	
Pyrex	-524	-107	

results in a TECs lower than that for exclusive B-site substitution. The support material for use in oxygen permeable membrane systems can not have oxygen permeability. Hence, for instance cobalt substituted $LaCrO_3$ must be excluded.

The effect of the difference in TEC between membrane and support on the membrane stress due to preparation (separate sealing) and *in situ* sealing is shown in Fig. 4a. The stress is linearly dependent on the difference in TEC. By assuming 100 MPa as a typical tensile strength of a membrane material and no relaxation of stress during the cooling process, the maximum difference in TEC to avoid cracking during preparation of the

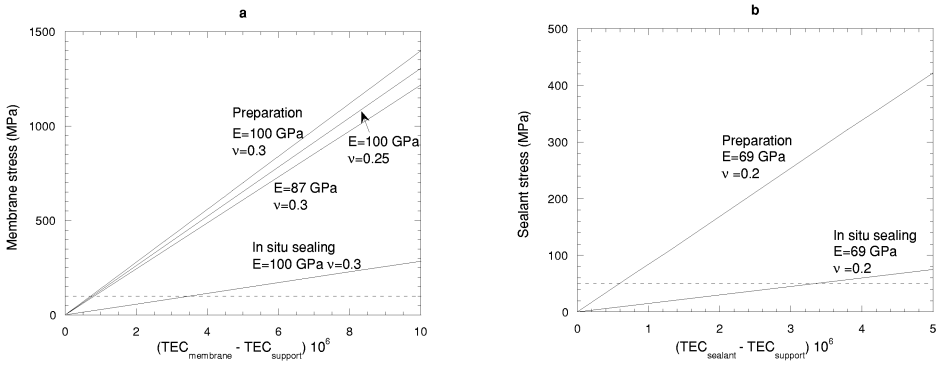

Figure 4: The effect of mismatch in TEC on the (a) membrane stress and (b) sealant stress due to preparation (ΔT=-980K) and *in situ* sealing (ΔT=-200K) of the membrane system (Fig. 3a,c).

membrane is $\sim 10^{-6}K^{-1}$ (Fig. 4a), assuming $\mathrm{TEC_{membrane}} > \mathrm{TEC_{support}}$. For the general case ($\mathrm{TEC_{membrane}}$ and $\mathrm{TEC_{support}}$ arbitrary) the permitted difference in TEC between membrane and support lies in the range $-10^{-5}K^{-1} < \Delta\mathrm{TEC} < 10^{-6}K^{-1}$, assuming compressive strength $\approx 10\cdot$ tensile strength. The effect of the difference in TEC between sealant and support on the sealant stress is shown in Fig. 4b. A typical bend strength of a sealing material (glass) is 69 MPa at room temperature [3]. Assuming 50 MPa as a typical tensile strength of a sealing material (glass), the permitted difference in TEC between sealant and support lies in the same range as for preparation (Fig. 4b). A similar consideration of *in situ* sealing gives rise to $\sim 3 \cdot 10^{-6}K^{-1}$ as the maximum differences in TEC between membrane / sealant and support not to build up a residual stress larger than 100 MPa and 50 MPa, respectively (Fig. 4a,b). Different Poisson's ratios and Young's moduli influence the stress nonlinearly. However, within the Poisson's ratios and Young's moduli of current interest, the influence on the stress is small (Fig. 4a).

It should be noted that in the simplified model (Eq. 10 and 11), where it is assumed that the membrane and sealant layers are much thinner than the support material, the stress in the membrane material is independent of which sealing material is chosen. Likewise, the stress build-up in the sealing material is independent of the membrane material. However, by assuming typical thicknesses for the different layers, $t_{membrane} = t_{sealant} = 100$ μm and $t_{support} = 10$ mm, and using the non-simplified equations (7) and (8), the difference from the simplified model for the membrane and the sealant

stresses are found to be <1%. As long as the assumption that the membrane and the sealant layers are much thinner than the support material is valid, the effect of layer thickness on the stress build-up in membrane and sealant is negligible.

Until now only stresses due to differences in thermal expansion have been considered. However, the overall expansion of an oxygen deficient material contains two components: one that is caused by the temperature and one that is caused by the change of oxygen stoichiometry (chemical expansion). Chemical expansion during cooling and heating the membrane system in air is included in the TECs (Table 1). However, during operation, the membrane may be exposed to a pO_2 of 10^{-19} atm at the syngas side and a pO_2 of 0.2 atm at the air side. Hendriksen et al. [43] found an overall expansion for $La_{0.6}Sr_{0.4}Co_{0.2}Fe_{0.8}O_{3-\delta}$ of 0.35% at operating conditions (800°C). By assuming 0.35% as a typical chemical expansion of a membrane material at operating conditions, the residual stress developed equals -500 MPa (ν=0.3, E=100 GPa). However, the membrane will be exposed to a residual stress before the membrane is in operation due to the cooling process from the sealing temperature (Fig. 3c). Stresses are in general additive. Thus, the 'total' build-up of stress in the membrane material due to thermal and chemical expansion during *in situ* sealing is included in Table 3, assuming no relaxation of stress and no cracking of the membrane material before operating conditions are set [2]. All membranes are in compression, and no cracking is expected to occur. It should be noted that the residual stress from chemical expansion contributes considerably to the 'total' build-up of stress for all membranes under consideration.

To find out if it is possible to prepare dense oxygen permeable membranes without doing *in situ* sealing, the relaxation times of the residual stresses due to the cooling process from sealing temperature, must be analyzed. The steady state creep rates of $La_{0.85}Sr_{0.15}MnO_{3+\delta}$ at 900°C and 800°C in air with a stress of 100 MPa are of the order 10^{-8} s^{-1} and 10^{-10} s^{-1}, respectively; extrapolated from creep data measured by Wolfenstine et al. [44]. Wolfenstine et al. also showed a slightly decreasing creep rate of $La_{1-x}Sr_xMnO_3$ with increasing Sr content. However, for 0.10<x<0.25 the steady state creep rate was observed to be of the same order of magnitude. $Sr_{1.05}FeO_3$ has been observed to have creep rates one order of magnitude larger than $La_{0.85}Sr_{0.15}MnO_{3+\delta}$ [45]. However, we assume 10^{-8} s^{-1} and

[2] To decrease the magnitude of the residual stress arising before operating conditions are set, the cooling process from sealing temperature to operating temperature could be done in a pO_2 gradient like under operating conditions.

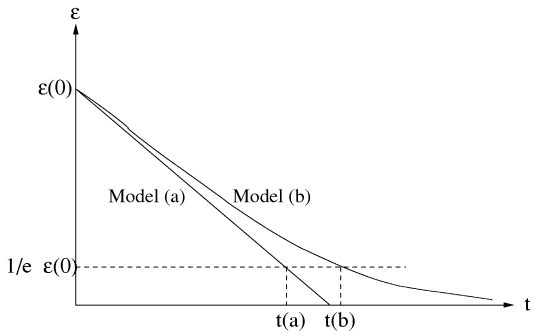

Figure 5: A schematic illustration of strain as a function of time for model (a) and model (b).

10^{-10} s^{-1} as typical creep rates for membrane materials at respectively 900°C and 800°C in air with a stress of 100 MPa.

In general, the steady state creep rate at a fixed oxygen partial pressure, can be represented by an equation of the form:

$$\frac{d\epsilon}{dt} = -A\sigma^n \exp\left(-\frac{Q}{RT}\right) \tag{16}$$

where A is a constant, σ is stress, n is stress exponent, Q is activation energy, R is the gas constant and T is absolute temperature [46]. This model assumes that the rate limiting mechanism for creep is independent of temperature. Due to the unknown relation between σ and ϵ, two limiting models will be considered: (a) assumes a constant residual stress, given as the maximum stress due to different thermal contraction in the temperature interval in question, $\sigma = \sigma_0$ (independent of strain); (b) assumes Hooke's law, $\sigma(\epsilon(t)) = \epsilon(t) \cdot E$. By using Eq. 16, model (a) gives rise to a linearly decreasing strain, $\epsilon(t) = \epsilon(0) - A\sigma_0^n \exp\left(-\frac{Q}{RT}\right) t$, and model (b) gives rise to an exponentially decreasing strain, $\epsilon(t) = \epsilon(0)\exp(-A^* t)$, $A^* = A\exp\left(-\frac{Q}{RT}\right) E$, assuming n=1. A schematic illustration of the two models is given in Fig. 5, showing ϵ as a function of t. Model (a) gives a relaxation time $\tau_a \sim \frac{\frac{1}{e}\epsilon(0)}{\frac{d\epsilon}{dt}}$, which is an underestimate of the true relaxation time. Model (b) gives rise to a relaxation time $\tau_b \sim \frac{1}{A^*}$, which is an overestimate. $\epsilon(0)$ is chosen as the strain obtained in the cooling process from sealing temperature when the residual stress equals 100 MPa (Eq.

10 with σ_1 = 100 MPa, ν_1 = 0.3 and E_1=100 GPa, giving $\epsilon(0)$=0.0007). Wolfenstine et al. [44] found the stress exponent for $La_{0.85}Sr_{0.15}MnO_3$ to be essentially independent of temperature and equal to 1.1±0.1. Thus, by using n=1, $\epsilon(0)$ = 0.0007 and Q=475 kJ/mole [44], the relaxation times in air at 900°C and 800°C with a residual stress of 100 MPa can be calculated and are shown in Table 4. The results reveal that within practical time scales, sealing has to be done *in situ* to avoid cracking of the dense oxygen permeable membranes under consideration.

Table 4: Relaxation times in air from 100 MPa at 800°C and 900°C.

	Membrane†		Sealant ($CaSiO_3$)	
	Model (a)	Model (b)	Model (a)	Model (b)
800°C	50 days	∼ years	2 h	7 h
900°C	12 h	50 days	1 s	5 s

† We assume that stress relief in the sealant does not influence the membrane stress.

Until now it has been assumed that stress relief in the sealant does not influence the membrane stress. However, in real membrane systems, viscous flow in the sealant may reduce the membrane stress. The viscosity, η, of a glass is well described by an equation of the Vogel-Fulcher form:

$$\eta = \eta_0 \cdot \exp\left(\frac{A}{T - T_0}\right) \tag{17}$$

where A, T_0 nd η_0 are material constants and T is absolute temperature. Over a narrow temperature range (∼ 50-100°C) [47], η may be represented by the equation:

$$\eta = \eta_0 \cdot \exp\left(\frac{Q}{RT}\right) \tag{18}$$

where Q is an activation energy and R is the ideal gas constant. Experimental data for $CaSiO_3$ ([48,49]) were least squares fitted to the Vogel-Fulcher equation, giving viscosities for use in Eq. 18. The activation energy, thus, obtained was of the order 900 kJ/mole. Dienes and Klemm [50] have found an expression relating viscosity and creep rate by using a parallel plate method. The geometric properties of their experimental setup is quite different from the present oxygen permeable membrane system. However, creep rate, stress and viscosity are generally related by

$$\frac{d\epsilon}{dt} \sim \frac{\sigma l}{\eta} \tag{19}$$

irrespective of geometry. Here l has dimension of length. In the present system the thickness of the sealant layer is the only relevant length scale. By setting l=100 μm, $\frac{d\epsilon}{dt}$ can be approximated by assuming equality in Eq. 19. Using σ = 100 MPa, both model (a) and model (b) [3] described in the preceding section give rise to relaxation times in the order of hours and seconds at 800°C and 900°C, respectively (Table 4). These results reveal a rapid relaxation of stress in $CaSiO_3$ glass above T_g. Thus, no residual stresses appear in the sealant ($CaSiO_3$) when performing *in situ* sealing because the operating temperature is higher than T_g. Rapid stress relief in the sealant causes a decreasing membrane stress, eventually zero. Thus, the build-up of residual stress in the membrane material depends on T_g of the sealant. Unlike most crystalline materials, however, glasses do not have fixed stoichiometry. Modifications of relative component concentrations are therefore permitted within certain limits, enabling design of glasses with suitable properties, e.g. T_g and TEC. The TEC is important since stresses may be accumulated below T_g, where the glass is rigid.

4 Conclusions

Residual stresses in oxygen permeable membrane systems have been calculated by using a model based on the force balance approach for general asymmetric composites, assuming the membrane and sealant layers are much thinner than the support material. The equations derived reveal that no stress appears in the support material. It is obvious that the difference in thermal expansion coefficient is the significant quantity for establishing a residual stress state. Thus, sealing and support materials with thermal expansion coefficients minimizing the stress could be designed. The ideal situation is $\alpha_{\text{membrane}} \approx \alpha_{\text{sealant}} \lesssim \alpha_{\text{support}}$. If we assume no relaxation of the residual stress and separate sealing of the membrane, the differences in TEC between membrane/sealant and support have to lie in the range $-10^{-5}K^{-1} < \Delta\text{TEC} < 10^{-6}K^{-1}$ to keep the stress below 100 MPa. The critical part of the preparation process is cooling the sealed membrane to room temperature due to long relaxation times of the residual stress in the membrane. To avoid cracking, *in situ* sealing of the membrane is necessary. The stress due to chemical expansion is shown to be of significant importance when performing *in situ* sealing of a typical membrane. Relaxation of residual stress in sealants having T_g below the operating temperature of

[3] The stress exponent, n, for viscous flow equals one.

the membrane (e.g. $CaSiO_3$), is found to occur almost instantly above the operating temperature. Hence, glass sealants with suitable T_g should be designed to minimize the build-up of residual stress in the membrane.

References

[1] G. P. Khattak and D. E. Cox, *Mat. Res. Bull.*, **12** 463 (1977).

[2] P. H. Larsen, P. V. Hendriksen and M. Mogensen, *J. Thermal Analysis*, **49** 1263 (1997).

[3] D. W. Richerson, *Modern Ceramic Engineering*, Marcel Dekker, Inc., New York, (1992).

[4] O. V. Mazurin, M. V. Strelsins and T. P. Shavaiko-Shavaikovskaya, *Handbook of Glass Data, Physical science data 15 A*, Elsevier, Amsterdam, (1983).

[5] J. E. Shelby, *J. Appl. Phys.*, **50** [12] 8010 (1979).

[6] Y. Teraoka, T. Nobunaga, K. Okamoto, N. Miura and N. Yamazoe, *Solid State Ionics*, **48** [3-4] 207 (1991).

[7] Y. Teraoka, H. M. Zhang, K. Okamoto and N. Yamazoe, *Mat. Res. Bull.*, **23** [1] 51 (1988).

[8] S. Faaland, M.-A. Einarsrud and T. Grande, Reactions between calcium and strontium substituted cobaltite ceramic membranes and calcium silicate sealing materials, S. Faaland, M.-A. Einarsrud, T. Grande, *Chem. of Mat.*, In print.

[9] S. C. Kunz and R. E. Loehman, *Adv. Ceram. Mat.*, **2** [1] 69 (1987).

[10] S. Timoshenko, *J. Opt. Soc. Amer.*, **11** 233 (1925).

[11] N. S. V. Damme, D. C. Nagle and S. R. Winzer, *Appl. Phys. Lett.*, **58** [25] 2919 (1991).

[12] C. D. Pionke and G. Wempner, *J. Appl. Mech.*, **58** 1015 (1991).

[13] S. Ho and Z. Suo, *J. of Appl. Mech.*, **60** 890 (1993).

[14] S. Suresh, A. E. Giannakopoulos and M. Olsson, *J. Mech. Phys. Solids*, **42** [6] 979 (1994).

[15] A. V. Virkar, J. L. Haung and R. A. Cutler, *J. Am. Ceram. Soc.*, **70** [3] 164 (1987).

[16] G. Dreier and S. Schmauder, *Scripta Metallurgica et Materialia*, **28** 103 (1993).

[17] G. Dreier, G. Elssner, S. Schmauder and T. Suga, *J. Mat. Sci.*, **29** 144 (1994).

[18] J. B. Wachtman, *Mechanical Properties of Ceramics*, John Wiley & Sons, Inc., New York, (1996).

[19] V. V. Kharton, E. N. Naumovich, P. P. Zhuk, A. K. Demin and A. V. Nikolaev, *Soviet Electrochemistry*, **28** [11] 1376 (1992).

[20] V. V. Kharton, L. Shuangbao, A. V. Kovalevsky and E. N. Naumovich, *Solid State Ionics*, **96** 141 (1997).

[21] K. Kleveland, M.-A. Einarsrud and T. Grande, Sintering behaviour, microstructure and phase composition of $Sr(Fe, Co)O_{3-\delta}$ ceramics, Accepted by *J. Am. Ceram. Soc.* (2000).

[22] K. Kleveland, M.-A. Einarsrud and T. Grande, *J. of European Ceram. Soc.*, **20** 185 (2000).

[23] V. V. Kharton, A. A. Yaremchenko, A. V. Kovalevsky, A. P. Viskup, E. N. Naumovich and P. F. Kerko, *J. Membrane Sci.*, **163** 307 (1999).

[24] S. Srilomsak, D. P. Schilling and H. U. Anderson, *Proceedings of The First Int. Symp. on Solid Oxide Fuel Cells*, Edited by S. C. Singhal, p. 129, (1989).

[25] E. Rencker, *C. R. Hebd. Seances Acad. Sci.*, **199** 1114 (1934).

[26] E. Rencker, *Bull. Soc. Chim. Fr.*, **2** 1389 (1935).

[27] N. P. Danilova, *Steklo*, **1** 89 (1967).

[28] N. P. Danilova and S. K. Dubrovo, *J. Appl. Chem. USSR (Engl. Transl.)*, **40** 959 (1967).

[29] D. L. Rothermel, *J. Am. Ceram. Soc.*, **50** 574 (1967).

[30] N. P. Bansal and R. H. Doremus, *Handbook of Glass Properties*, Academic Press, Inc., New York, (1986).

[31] K. Suganuma, T. Okamoto, M. Koizumi and M. Shimada, *Comm. of the Am. Ceram. Soc.*, **Dec.** C-256 (1984).

[32] N. Orlovskaya, K. Kleveland, T. Grande and M.-A. Einarsrud, *J. European Ceram. Soc.*, **20** 51 (2000).

[33] C. M. D'Souza, *J. Am. Ceram. Soc.*, **83** [1] 47 (2000).

[34] Y.-S. Chou, J. W. Stevenson, T. R. Armstrong and L. R. Pederson, *J. Am. Ceram. Soc.*, **83** [6] 1457 (2000).

[35] B. L. Cheng, M. Gabbay, W. Duffy and G. Fantozzy, *J. Mater. Sci.*, **31** 4951 (1996).

[36] J. M. Blamey and T. V. Parry, *J. Mater. Sci.*, **28** 4317 (1993).

[37] C. S. Montross, H. Yokokawa, M. Dokiya and L. Bekessy, *J. Am. Ceram. Soc.*, **78** [7] 1869 (1995).

[38] J. Drennan, V. Zelizko, D. Hay, F. T. Ciacchi, S. Rajendran and S. P. S. Badwal, *J. Mater. Chem.*, **7** [1] 79 (1997).

[39] S. Baskaran, C. A. Lewinsohn, Y.-S. Chou, M. Quian, J. W. Stevenson and T. R. Armstrong, *J. Mater. Sci.*, **34** 3913 (1999).

[40] S. W. Paulik, S. Baskaran and T. R. Armstrong, *J. Mater. Sci.*, **33** 2397 (1998).

[41] N. M. Sammes and R. Rataraj, *J. Mater. Sci.*, **29** 4319 (1994).

[42] S. Faaland, G. Stakkestad, A. Bardal, T. Sigvartsen and R. Høier, *Proceedings of the 17th Risø International Symposium on Materials Science: High Temperature Electrochemistry: Ceramics and Metals*, Roskilde, Denmark, Edited by F. W. Paulsen, N. Bonanos, S. Linderoth, M. Mogensen and B. Zachau-Christiansen, p. 241, (1996).

[43] P. V. Hendriksen, P. H. Larsen, M. Mogensen, F. W. Poulsen and K. Wiik, *Catalysis Today*, **56** 283 (2000).

[44] J. Wolfenstine, K. C. Goretta, R. E. Cook and J. L. Routbort, *Solid State Ionics*, **92** 75 (1996).

[45] K. Kleveland, A. Wereszczak, T.P. Kirkland, M.-A. Einarsrud, T. Grande, Submitted to *J. Am. Ceram. Soc.* (2000).

[46] F. H. Norton, *The creep of steel at high temperature*, McGraw Hill, New York, (1929).

[47] C. J. Brinker and G. W. Scherer, *Sol-Gel Science*, Academic Press, Inc., San Diego, p. 679 (1990).

[48] J. O. Bockris and D. C. Lowe, *Proc. R. Soc. Ser. A, 226, 1167*, London, p. 423, (1954).

[49] B. G. Varshal, V. Y. Goikhman, L. L. Mirskikh, L. K. Shitts and Y. A. Shitts, *Fiz. Khim. Stekla*, **6** [6] 734 (1980).

[50] G. J. Dienes and H. F. Klemm, *J. Appl. Phys.*, **17** 458 (1946).